Computer Assisted Mechanics and Engineering Sciences, 12: 299–328, 2005.

Numerical analysis of a reinforced concrete beam and a deep beam under impulsive loading

Adam Stolarski and Waldemar Cichorski
Military University of Technology,
Kaliskiego 2, 00-908 Warsaw-49, Poland

(Received January 23, 2003)

An analysis of the dynamic behaviour of a reinforced concrete beam and a deep beam taking into account the physical non-linearities of structural materials is presented in this paper. The modified model of the elastic/visco-perfectly plastic material with regard to delayed yield effect was applied to the reinforcing steel. The non-standard model of dynamic deformation was applied to the concrete. The model describes the elastic properties until attaining the dynamic strength of concrete, perfectly plastic properties in the limited range of deformation, material softening, and smeared cracking or crushing which are concentrated in the regions of the tensile or compressive residual stress states. Interaction between the reinforcing steel and the concrete is conditioned by the assumption of perfect consistency of displacements of both materials. The ratio of this interaction depends on the phase of deformation of the concrete. The method of analysis of the structural system was developed using the finite element method. The results of numerical solutions are presented. The effectiveness of the method of analysis and computational algorithms for problems of numerical simulation of the reinforced concrete beam and the deep beam dynamic behaviour is indicated in this paper.

Keywords: R/C deep beam, physical non-linearity, dynamics, numerical analysis

1. Introduction

There are a few well known papers from the range of modelling of dynamic behaviour of R/C structures in the literature. Nonlinear wave propagation in reinforced concrete structures was studied in monograph [18]. Numerical analysis of reinforced beams under impact loads was described in paper [8]. Dynamically loaded beams and square plates were analysed in paper [17]. Cantilevers and fully clamped beams under impulsive loading ware analysed in paper [10]. Some new solutions concerning the dynamic response of plain concrete structures type of dam were proposed in papers [11, 12].

The aim of this paper is the analysis of dynamic behaviour of reinforced concrete beams and reinforced concrete deep beams taking into account the physical non-linearities of structural materials, *i.e.* concrete and reinforcement steel. In order to obtain the solutions to the problem, the considerations in the range of the modelling of inelastic material properties and modelling of deformation processes of the plane structural element together with the elaboration of numerical solutions were carried out.

The present paper is a further development of the theory presented by the authors in paper [5]. Introductory results of the analysis in the range discussed in the present paper were analysed in paper [22].

Analysis of the deformation processes, which are carried out at high rates, requires taking into consideration the dynamic material properties. The modified model of the elastic/visco-perfectly plastic material with regard to the delayed yield effect was applied to the reinforcement steel, [1]. The non-standard model of dynamic deformation was applied to the concrete, [21]. The basis of this model is the method of determination of the initial dynamic yield surface. For this purpose,

the structure of Campbell's dynamic yield criterion was used, [4]. The proposed criterion is an integral condition of attaining the dynamic strength. The calculated dynamic strength is treated as a parameter in the constitutive equations, which describe the elastic-plastic model of concrete. The model describes the effect of increase of the dynamic strength in proportion to static strength, limited perfectly plastic properties of concrete, material softening and material dilatation in the straining process. Degradation of elastic material constants was disregarded and the unloading processes are linear and elastic. The assumption of such a concrete model enables the simplified description of cracking or crushing of material as the states of loss of load capacity, which are reached in the material softening process during tension or compression.

The method of analysis of the structural system was developed using the finite element method, [13, 25]. The hypothesis of interaction between reinforcement bars and concrete was proposed. The system of the FEM incremental equilibrium equations was solved on the basis of algorithms and procedures of numerical analysis of the plane stress state problem. The solution enables the determination of displacement, strain, and stress states with regard to the structural materials sensitivity to the strain rate and physical non-linearities, including cracking processes in concrete.

The selected results of the numerical solutions are presented in this paper. The comparative analysis of the theoretical results with experimental results [8] and other theoretical results [2] are presented for the example of the reinforced concrete beam. The influence of the reinforcement ratio on the dynamic load-carrying capacity and character of the dynamic deformation process of the reinforced concrete deep beam was examined.

2. Dynamic model of reinforcement steel

The modified model of elastic/visco-perfectly plastic material taking into consideration the delayed yield effect was applied to dynamic analysis, [1]. Considering the reinforcement of the deep beam as slender steel bars, the deformation model in uniaxial stress state was applied to the reinforcement steel. In this model, Perzyna's constitutive equations of elastic-viscoplasticity [19], can be written in the form

$$\dot{\varepsilon} = \frac{\dot{\sigma}}{E_a} + \tilde{\gamma} < \Phi(F) > , \qquad \tilde{\gamma} = \frac{2}{\sqrt{3}}\gamma , \tag{1}$$

where E_a – modulus of elasticity, γ – viscosity coefficient.

The modification of Perzyna's constitutive equations is based on the integration of those equations with the initial condition of the dynamic yield limit, which is determined on the base of Campbell's dynamic yield criterion [4], in the form

$$\int_0^{t_d} \left[\frac{\sqrt{\sigma(t)}}{R_a} \right]^{\alpha} \mathrm{d}t = t_0 , \tag{2}$$

where α and t_0 – material constants, R_a – tensile-compressive strength of steel.

At the instant of satisfying Campbell's criterion, time of delayed yielding $t = t_d$ and dynamic yield limit $R_{ad} = \sigma(t_d) \geq R_a$, are determined.

Static yield function for the elastic-perfectly plastic material has the form

$$F = \frac{\sigma}{R_a} - 1 . \tag{3}$$

Symbol $< \Phi(F) >$ is defined as follows

$$< \Phi(F) >= \left\{ \begin{array}{lll} 0 & & \text{for } t \leq t_d \\ \Phi(F) & \text{if} \quad F > 0 & \\ 0 & \text{if} \quad F \leq 0 & \end{array} \right\} \quad \text{for } t > t_d . \tag{4}$$

Nonlinear function $\Phi(F)$, was assumed in the form of a power law

$$\Phi(F) = F^{\delta}, \tag{5}$$

where δ – material coefficient.

Dynamic yield condition, has the form

$$\sigma = R_a \left[1 + \left(\frac{\sqrt{\dot{\varepsilon}^{vp}}}{\tilde{\gamma}} \right) \right]^{\delta^{-1}}, \tag{6}$$

where $\dot{\varepsilon}^{vp}$ – viscoplastic strain rate.

3. Dynamic model of concrete

The non-standard model of dynamic deformation of concrete was applied in the dynamic analysis, [21]. The basic elements of the model are presented in the following.

Limit surface equation depending on I_1 – the first invariant of stress tensor σ_{ij} and J_2, J_3 – the second and the third invariants of stress deviator s_{ij}, $i, j, k = 1, 2, 3$ is assumed in the following form

$$F(\sigma_{ij}) = \left[\frac{\tau_0}{\rho(\varphi)} + a \right]^2 - b\sigma_0 - c = 0, \tag{7}$$

where $\tau_0 = \sqrt{2J_2/3}$ – tangent octahedral stress, $\sigma_0 = I_1/3$ – mean normal stress, a, b, c – material constants, depending on basic, static strengths of concrete for uniaxial and biaxial compression and uniaxial tension.

Function $\rho(\varphi)$, determining the shape of the limit surface cross-section by the octahedral plane $\sigma_0 = \text{const}$, is assumed in the form proposed by Willam and Warnke [24]

$$\rho(\varphi) = \frac{2(1-\lambda^2)\cos\left(\frac{\pi}{3} - \varphi\right) + (2\lambda - 1)\sqrt{4(1-\lambda^2)\cos^2\left(\frac{\pi}{3}\right) + 5\lambda^2 - 4\lambda}}{4(1-\lambda^2)\cos^2\left(\frac{\pi}{3} - \varphi\right) + (2\lambda - 1)^2} \tag{8}$$

where φ – angle depending on stress state

$$\cos 3\varphi = \sqrt{2}\frac{J_3}{\tau_0^3}. \tag{9}$$

Parameter λ determines the relation between characteristic values of radius $\rho(\varphi)$ for uniaxial tension or biaxial compression $\rho_t = \rho(\varphi = \pi/3) = \lambda$ and for uniaxial compression $\rho_c = \rho(\varphi = 0) = 1$

$$\lambda = \frac{\rho_t}{\rho_c}, \tag{10}$$

and can be admitted as the material feature.

Constant value of parameter λ, determining the so-called tension curve in equation of limit surface, was assumed on the base of Reimann's definition [20]

$$\lambda = \frac{3\,r_{cc}\,r_t + r_{cc} - r_t}{2\,r_{cc} - r_t}, \tag{11}$$

where non-dimensional static strengths of concrete

$$r_t = \frac{R_t}{R_c}, \qquad r_{cc} = \frac{R_{cc}}{R_c}, \qquad r_c = \frac{R_c}{R_c} = 1, \tag{12}$$

are determined by R_c, R_t, R_{cc} – static strengths of concrete for uniaxial compression, uniaxial tension, and biaxial compression obtained from experimental data.

Material constants a, b, and c can be determined on the base of experimental static tests for uniaxial and biaxial compression and uniaxial tension in the following forms

$$a = \frac{\sqrt{2}}{6} \frac{\left[1 - \left(\frac{r_t}{\lambda}\right)^2\right](2r_{cc} - 1) - \left[\left(\frac{r_{cc}}{\lambda}\right)^2 - 1\right](r_t + 1)}{\left(\frac{r_{cc}}{\lambda} - 1\right)(r_t + 1) - \left(1 - \frac{r_t}{\lambda}\right)(2r_{cc} - 1)},$$

$$b = \frac{\frac{2}{3}\left[1 - \left(\frac{r_t}{\lambda}\right)^2\right] + 2\sqrt{2}\left(1 - \frac{r_t}{\lambda}\right)a}{r_t + 1}, \qquad c = \left(\frac{\sqrt{2}}{3} + a\right)^2 - \frac{1}{3}b, \tag{13}$$

The basis of the model is the method of attaining the initial dynamic yield surface. For this purpose, the integral criterion of dynamic strength for concrete in complex stress states, was proposed

$$\int_0^{t_d} [\psi(t)]^{\alpha_c} \mathrm{d}t = t_{c0}, \tag{14}$$

where $\psi(t)$ is determined on the base of static limit surface according to equation (7) as follows

$$\psi(t) = \frac{2\left[\frac{\tau_0}{\rho(\varphi)}\right]^2}{2a\frac{\tau_0}{\rho(\varphi)} - b\sigma_0} \left\{ \sqrt{1 - \frac{4(a^2 - c)\left[\frac{\tau_0}{\rho(\varphi)}\right]^2}{\left[2a\frac{\tau_0}{\rho(\varphi)} - b\sigma_0\right]^2}} - 1 \right\}^{-1}, \tag{15}$$

and α_c and t_{c0} are material constants, which are determined on the base of experimental results for concrete.

At the instant $t = t_d$ of satisfying the criterion of dynamic strength (14), dynamic strength coefficient of concrete is determined

$$\psi_d = \psi(t_d) \geq 1. \tag{16}$$

Properties of the limit surface, especially its good agreement with experimental results for concrete in complex stress states, give the reason for applying Eq. (7) as a yield surface for the elastic-plastic material, in the following form

$$F(\sigma_{ij}, K) = \left[\frac{\tau_0}{\rho(\varphi)} + Ka\right]^2 - Kb\sigma_0 - K^2 c = 0. \tag{17}$$

Parameter K has the meaning of the scaling parameter for the basic strength of concrete and, on the other hand, can be interpreted as the evolution parameter for the dynamic yield surface in the stress space.

The following relation of the evolution parameter is assumed

$$K = \begin{cases} 1 & & t < t_d \\ \psi_d & \varepsilon^p_{ef} \le \varepsilon^p_R & t \ge t_d \\ \psi_d + \int\limits_{t_R}^{t} \dot{K}(\tau)\mathrm{d}\tau & \varepsilon^p_{ef} > \varepsilon^p_R & t > t_d \\ K_m & \varepsilon^p_{ef} = \varepsilon^p_u & t > t_d \\ 0 & \varepsilon^p_{ef} > \varepsilon^p_u & t > t_d \end{cases} , \tag{18}$$

where ε^p_{ef} – effective plastic strain, ε^p_R – limit plastic strain in the perfect plastic flow phase, ε^p_u – limit plastic strain in the material softening phase, $t_R = t(\varepsilon^p_R)$ – the end instant of perfectly plastic flow and commencement of the material softening phase, K_m – minimum value of the evolution parameter determining the end of the material softening phase and initiation of the failure phase: cracking (for tension) or crushing (for compression) of concrete.

The applied definition of the evolution parameter K describes the four-phase idealisation of concrete behaviour. The following deformation phases are distinguished in this idealisation:

1) elastic state until attaining the initial yield surface,

2) perfectly plastic flow in limited range of deformation,

3) material softening modelled as plastic flow on the transient yield surface, the isotropic shrinkage process which is controlled by variation $\dot{K}$ of the evolution parameter, depending on the effective plastic strain rate and softening modulus and modified interdependence on the transient stress state,

4) residual (stress free) state.

Interpretation of the evolution parameter K corresponding to four-phase approximation of concrete behaviour for the uniaxial compression is presented in Fig. 1.

The following relation describes variation $\dot{K}$ of the evolution parameter

$$\dot{K} = \begin{cases} 0 & \text{if} \quad \varepsilon^p_{ef} \le \varepsilon^p_R \\ \psi_d H(\sigma^0_i)\,\dot{\varepsilon}^p_{ef} & \text{if} \quad \varepsilon^p_{ef} > \varepsilon^p_R \\ 0 & \text{if} \quad \varepsilon^p_{ef} > \varepsilon^p_u \end{cases} , \tag{19}$$

where $\dot{\varepsilon}^p_{ef}$ – effective plastic strain rate, $H(\sigma^0_i)$ – material softening modulus.

Non-dimensional material softening modulus has the form

$$H(\sigma^0_i) = -\frac{1}{\sigma^0_i(\varepsilon_{uc} - \varepsilon_{Rc} + \varepsilon^e_c)} , \qquad \varepsilon^e_c = \frac{R^d_c}{E_c} , \qquad R^d_c = \psi_d R_c , \tag{20}$$

where σ^0_i – non-dimensional stress intensity related to initial yield surface, ε_{Rc} and ε_{uc} – limit plastic strains, E_c – modulus of elasticity.

Value of the softening modulus depends on the stress state in proportion to non-dimensional stress intensity

$$\sigma^0_i = s(t)\sigma_i(t) , \qquad s(t) = \frac{1}{\psi(t)} , \tag{21}$$

related to static yield surface $F(\sigma^0_{ij}, K = 1) = 0$.

Limit plastic strains ε^p_R and ε^p_u for the perfectly plastic flow phase and for the material softening phase are taken in the forms

$$\varepsilon^p_R = \sigma^{0d}_i(\varepsilon_{Rc} - \varepsilon^e_c) , \qquad \varepsilon^p_u = \sigma^{0d}_i(\varepsilon_{Kc} - \varepsilon^e_c) , \qquad \varepsilon_{Kc} = \varepsilon_{uc} - \frac{K_m}{\psi_d}(\varepsilon_{uc} - \varepsilon_{Rc}) , \tag{22}$$

where $\sigma^{0d}_i = \sigma^0_i(t_d)$ is determined for the instant $t = t_d$ of dynamic strength criterion fulfilment.

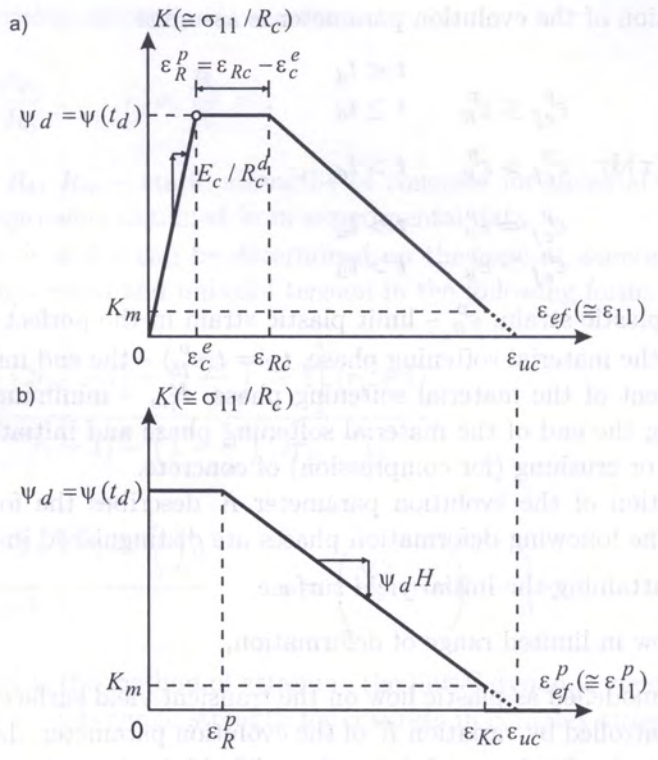

Fig. 1. Interpretation of the evolution parameter: a) for total strain values of effective strain, b) for plastic strain components of effective strain

The basic values of the limit strains ε_{Rc} and ε_{uc} are taken as the constant values, independent of grade of concrete and strain rate from the analysis of the experimental results for uniaxial compression

$$\varepsilon_{Rc} = 0.002\ , \qquad \varepsilon_{uc} = 0.006 \div 0.012\ , \tag{23}$$

where lower values of ε_{uc} may be used for high-grade concrete and higher values for low- and mean-grade concrete.

Effective plastic strain ε_{ef}^p is defined as follows

$$\varepsilon_{ef}^p(t) = \int_{t_d}^{t} \dot{\varepsilon}_{ef}^p(\tau)\mathrm{d}\tau\ . \tag{24}$$

In turn, effective plastic strain rate $\dot{\varepsilon}_{ef}^p$ is assumed as the modified form of plastic strain rate intensity in which the influence of transverse strains is neglected

$$\dot{\varepsilon}_{ef}^p = \dot{\varepsilon}_i^p(\nu_c = 0) = \sqrt{\frac{3}{2}}\sqrt{\dot{e}_{ij}^p(\nu_c = 0)\dot{e}_{ij}^p(\nu_c = 0)}\,, \tag{25}$$

where $\dot{e}_{ij}^p$ – components of plastic strain rate deviator.

Tensor of the plastic strain increment is defined by the non-associated flow rule

$$\dot{\varepsilon}_{ij}^p = \dot{\Lambda}\frac{\partial G}{\partial \sigma_{ij}}\ , \tag{26}$$

with the assumption of the elastic-plastic strain rates decomposition

$$\dot{\varepsilon}_{ij} = \dot{\varepsilon}_{ij}^e + \dot{\varepsilon}_{ij}^p\ . \tag{27}$$

Plastic potential function G was assumed in the form of a modified yield surface function

$$G(\sigma_{ij}, K) = \left[\frac{\tau_0}{\rho(\varphi)} + Ka\right]^2 - K\frac{b}{\beta}\sigma_0 - K^2 c = 0\,, \tag{28}$$

where β – material constant defining the volumetric variation of the material during plastic deformation.

Linear-elastic material properties are described by generalised Hooke's law which, taking into account the strain increments decomposition and flow rule, can be written in the form

$$\dot{\sigma}_{ij} = C_{ijkl}\dot{\varepsilon}^e_{kl} = C_{ijkl}\left(\dot{\varepsilon}_{kl} - \dot{\varepsilon}^p_{kl}\right) = C_{ijkl}\left(\dot{\varepsilon}_{kl} - \dot{\Lambda}\frac{\partial G}{\partial \sigma_{kl}}\right)\,, \tag{29}$$

where C_{ijkl} – elastic constants tensor.

Loading parameter is determined on the base of the relation

$$\dot{\Lambda} = \frac{\dfrac{\partial F}{\partial \sigma_{ij}} C_{ijkl}\dot{\varepsilon}_{kl}}{\dfrac{\partial F}{\partial K}A(\psi_d, H, \eta_{ef}) + \dfrac{\partial F}{\partial \sigma_{ij}} C_{ijkl}\dfrac{\partial G}{\partial \sigma_{kl}}}\,, \tag{30}$$

where $A(\psi_d, H, \eta_{ef}) = -\psi_d H\left(\sigma_i^0\right)\eta_{ef}\left(\dfrac{\partial G}{\partial \sigma_{ij}}\right)$, $\eta_{ef} = \sqrt{\frac{3}{2}}\sqrt{\eta_{ij}\eta_{ij}}$, $\eta_{ij} = \dfrac{\partial G}{\partial \sigma_{ij}}$.

Loading and unloading processes are defined in the following way

$$\begin{array}{lllllll} \text{loading:} & \dot{\Lambda} > 0 & \text{if} & F = 0 & & \text{and} & \dot{F} = 0, \\ \text{unloading:} & \dot{\Lambda} = 0 & \text{if} & F < 0 & \text{or} \quad F = 0 & \text{and} & \dot{F} < 0. \end{array} \tag{31}$$

Applied deformation model of concrete enables the simplified modelling of the failure mechanism. This mechanism results from the applied softening rule, which assumes gradual loss of material load-capacity until attaining the residual stress state during the tension or compression processes.

Three different states of the failure mechanism can be defined at the moment of attainment of the minimal (residual) value of the evolution parameter

$$\begin{array}{ll} K_{mt} = K_m & \left\{ \begin{array}{lll} \text{if} & \sigma_0 < 0 & \text{cracking state} \\ \text{if} & 0 < \sigma_0 < \sigma_0^* & \text{semi} - \text{failure state}\,, \\ \text{if} & \sigma_0 \geq \sigma_0^* & \text{crushings state} \end{array} \right. \\ K_{mc} = K_{mt} = K_m & \end{array} \tag{32}$$

where σ_0^* is the conventional value of mean normal stress which can be assumed as $\sigma_0^* = 0.25 \cdot K \cdot R_c$.

The cracking state can be attained in the monotonic tension process or in the cyclic, convertible unloading from the compression process that reverses the loading in the tension process. The cracking state does not reduce the compression strength, and the reloading process in compression is possible after closing the generalised, volumetric crack.

The crack opening and closing mechanisms are determined by the following conditions

$$\begin{array}{l} \varepsilon_0 < \varepsilon_0^* \;-\; \text{crack opening}\,, \\ \varepsilon_0 \geq \varepsilon_0^* \;-\; \text{crack closing}\,, \end{array} \tag{33}$$

where ε_0^* is the last converged limit volumetric strain corresponding to the instant of attainment of the residual stress state in the tension process. In general, ε_0^* is not equal to zero due to its character as the plastic permanent strain in the elastic-plastic model of concrete.

The semi-failure state, being analogical to the cracking state, is characterised by it's capability to repeated commencement of the compression process if the current volumetric deformation is greater

than the limit volumetric strain $\varepsilon_0 \geq \varepsilon_0^*$, attained at the instant of the semi-failure state of concrete in the previous cycle of deformation.

The crushing state determines the total loss of stress carrying capacity of the concrete.

Assumed interpretation of cracking and crushing mechanism can be described by means of the indicator defined as the unitary, active cross-section of concrete

$$\delta = \begin{cases} \delta_c & \text{if} \quad \sigma_0 \geq 0 \,, \\ \delta_c \delta_t & \text{if} \quad \sigma_0 < 0 \,, \end{cases} \tag{34}$$

where $\delta_c = 1$ and $\delta_t = 1$ are initial values of the partial indicators that change their values only once, just at the moment when the residual stress states are attained

$$\begin{aligned} &\delta_c = 0 \quad \text{if} \quad K_{mc} = K_m \,, \\ &\delta_t = 0 \quad \text{if} \quad K_{mt} = K_m \,. \end{aligned} \tag{35}$$

Assuming that indicator δ determines the evolution parameter and the stress state in concrete as follows: $\tilde{K} = \delta K$ and $\tilde{\sigma}_{ij} = \delta \sigma_{ij}$, the stress free state $\tilde{\sigma}_{ij} = 0$, is determined directly by the indicator value $\delta = 0$ attained in the crushing process of the concrete $\delta_c = 0$ or in the cracking (or semi-failure) process $\delta_t = 0$.

4. Method of analysis

4.1. General description of the method

The solution was obtained on the basis of the method of analysis of the inelastic behaviour of the reinforced concrete deep beam under dynamic load, [23].

The method of structure analysis is based on: 1° discretisation and description of the structure according to the finite element method principles, [13, 25]; 2° formulation of the system of the incremental equilibrium equations; and 3° elaboration of own algorithms and procedures of numerical analysis of the plane stress state problem, which enable the determination of the displacement, strain, and nonlinear stress fields, both in reinforcement steel and concrete.

Assumed order of the constitutive equations for the concrete matrix material enables the tracing of the material softening phenomena with regard to the cracking and crushing processes in the areas of the critical stress states of the reinforced concrete structure.

4.2. Discrete model of reinforced concrete structure

The discretisation of the structure using FEM is based on the following assumptions.

1° The structure was divided into the finite elements of the matrix material (concrete) and of the reinforcement bars material (slender steel bars discretely distributed in the matrix material).

2° The natural for reinforced concrete structures hypothesis of the interaction between concrete and reinforcement steel was applied under the assumption of perfect consistency of the displacements of both materials.

The matrix material was divided into rectangular elements. Four-node elements with two degrees of freedom in each node were applied. A fine mesh was used in the regions in which concentration of stresses was expected.

The reinforcement steel bars were modelled as linear bar elements. Two-node elements with two degrees of freedom in each node were used.

In turn, the principle of concrete and reinforcement steel bars interaction is realised in the following way.

1° Two types of nodes are introduced:

- the main element nodes, respectively to the applied structure discretisation, distinguishing between the nodes of the matrix material elements and the nodes of the reinforcement bar material elements,
- the common nodes of the matrix material elements and the reinforcement bar material elements as selected from among the main nodes.

2° Displacement equivalence condition is introduced in the main nodes exclusively.

3° The computational Gauss points on the matrix material element area are introduced. This enables a full strain and stress state analysis and, in addition, to distinguish between tensile and cracking states inside the simple matrix material element, in addition to modelling of the reinforcement steel and concrete interaction within the tensile and cracked areas. The ratio of this interaction is determined by the phase of deformation of the concrete: from perfect bonding for the elastic and perfectly plastic stress states to the quasi-perfect slip for the tensile residual stress states.

4.3. System of equilibrium equations

The governing equation system for the solution of the dynamic problem of a reinforced concrete deep beam is determined in the following matrix and incremental form

$$M\ddot{r}_{t+\Delta t} + K\Delta r_{t,t+\Delta t} = R_{t+\Delta t} - F_t, \tag{36}$$

where M – mass matrix, $K = K_c + K_s$ elastic stiffness matrix which has the additive form consisting of stiffness matrices for concrete elements K_c and for reinforcement steel elements K_s, $\Delta r_{t,t+\Delta t}$ – unknown increment of the generalised displacement vector.

Unknown values of displacements, displacement rates and accelerations at the following instants t, $t + \Delta t$, are determined by the incremental expressions

$$r_{t+\Delta t} = r_t + \Delta r_{t,t+\Delta t}, \qquad \dot{r}_{t+\Delta t} = \dot{r}_t + \Delta \dot{r}_{t,t+\Delta t}, \qquad \ddot{r}_{t+\Delta t} = \ddot{r}_t + \Delta \ddot{r}_{t,t+\Delta t}. \tag{37}$$

The vector of generalised external loading is determined in the analogical, incremental way

$$R_{t+\Delta t} = R_t + \Delta R_{t,t+\Delta t}. \tag{38}$$

In turn, the vector of generalised nodal forces, which corresponds to stress state at the instant $t + \Delta t$, has the form

$$F_t = R_t - M\ddot{r}_t \equiv F_{t-\Delta t} + \Delta F_{t-\Delta t,t}, \qquad \Delta F_{t-\Delta t,t} = \int_V B^T \Delta \sigma_{t-\Delta t,t} \mathrm{d}V. \tag{39}$$

The system of equations of motion (36) is solved by means of the implicit numerical integration procedure, known as the Newmark method. Using this procedure enables the iterative solving of equations system with application of the modified Newton-Raphson method. In this method, a single triangularisation of stiffness matrix K, which is constant during the loading process in each time step, is used.

5. Numerical analysis of R/C beam

Numerical analysis was carried out for the reinforced concrete beams, which were subjected to experimental and numerical investigations by Emrich et al., [8].

Experimental results for the reinforced concrete beam denoted in paper [8] as TEST 115 was taken as the base of the comparative analysis.

The following data were introduced into the numerical analysis.

1° Simply supported beam under concentrated force at midspan, Fig. 2.

2° Geometrical parameters.

- Effective span of the beam: $L = 3.20$ m.
- Dimensions of the cross-section: $b = 0.25$ m, $h = 0.27$ m.
- Reinforcement in bottom layer: $A_s(4\phi 14) = 6.16$ cm^2.
- Reinforcement in upper layer: $A_{sc}(4\phi 10) = 3.14$ cm^2.

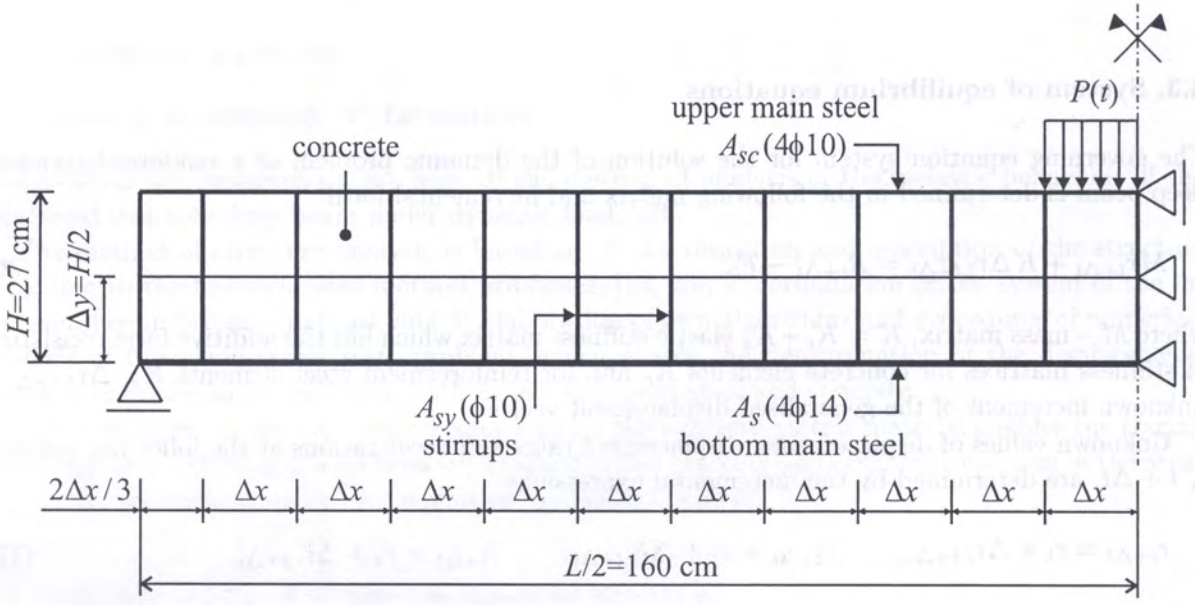

Fig. 2. Reinforced concrete beam under loading

3° Force-time function according to Fig. 3.

4° Material parameters.

- Mass density: $\rho = 2400$ kg/m^3.
- Concrete:

– static compressive strength: $R_c = 41$ MPa,

– elastic modulus: $E_c = 39$ GPa,

– constants in dynamic strength criterion: $\alpha_c = 17.75$, $t_{c0} = 0.180$ s,

– limit plastic strains: $\varepsilon_{Rc} = 0.002$, $\varepsilon_{uc} = 0.012$.

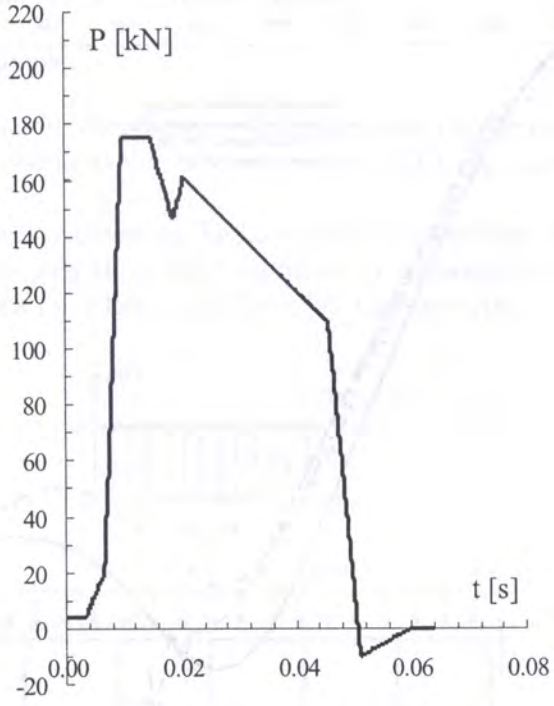

Fig. 3. Force-time function

- Reinforcement steel BSt 420/500 RK (according to German Code, see [8, 15]):

– tensile-compressive strength: $R_a = 420$ MPa,

– elastic modulus: $E_a = 210$ GPa,

– viscosity coefficient: $\gamma = 1.0 \cdot 10^6$ s^{-1},

– exponent coefficient in $\Phi(F)$ power function: $\delta = 13$,

– constants in dynamic yield criterion: $\alpha = 16.8$, $t_0 = 2.818$ s.

5° Finite element mesh of the beam in accordance with Fig. 1. One half of the calculated beam, considering symmetry of loading and structure, is shown in this figure.

For TEST 115, the comparison of computed variations in time of displacements (Fig. 4) and velocities (Fig. 5) in the midspan of the beam is presented.

As can be seen in Fig. 4, the displacements at midspan indicate good agreement with experimental results according to Emrich et al. [8] until attaining the fracture of the bottom reinforcement steel observed in the experiment at time instant $t \cong 0.06$ s. In the presented modelling of reinforced concrete beam behaviour, precise simulation of this phenomenon was not carried out. In turn, comparison with numerical results obtained, on the one hand, by Emrich et al. [8] by means of the finite element method using ADINA code, and, on the other hand, obtained by means of the finite difference method by Bąk and Stolarski [2], also show quite good quantitative agreement of the results.

The calculated velocity at the midspan of the beam is shown in Fig. 5, corresponds to the test results. Velocity – time relation was obtained in the paper of Emrich [8] by derivation of the measured displacement – time function. Comparison with numerical results obtained by means of the finite difference method by Bąk and Stolarski [2] shows good agreement of results.

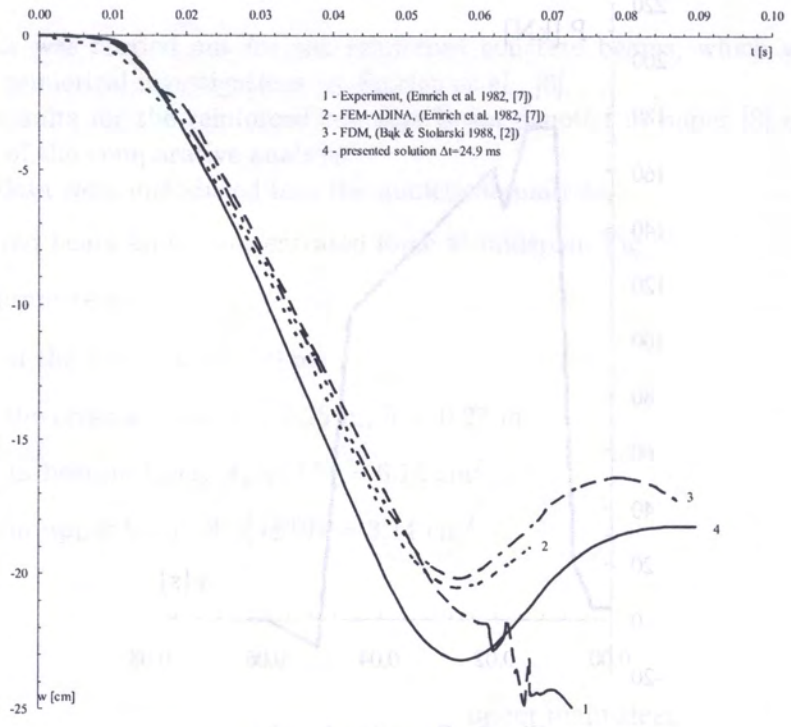

Fig. 4. Midspan displacement – time relation

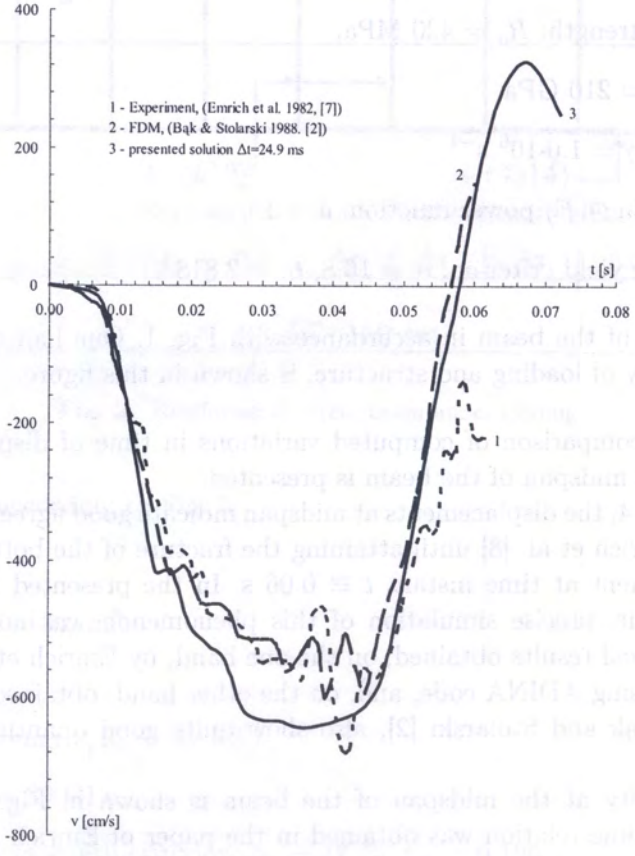

Fig. 5. Midspan velocity – time relation

6. Numerical analysis of R/C deep beam

6.1. The subject of analysis

Rectangular reinforced concrete deep beam with orthogonal reinforcement system, marked in the report by Leonhardt and Walther [14] as a test specimen WT3, was selected for numerical analysis, Fig. 6.

Static experimental results, carried out by Leonhardt and Walther, are often used as benchmark results for comparison with own theoretical solutions by different authors, e.g. by Cichorski and Stolarski [6, 7], Buyukozturk [3], Floegl and Mang [9], Lewiński [16].

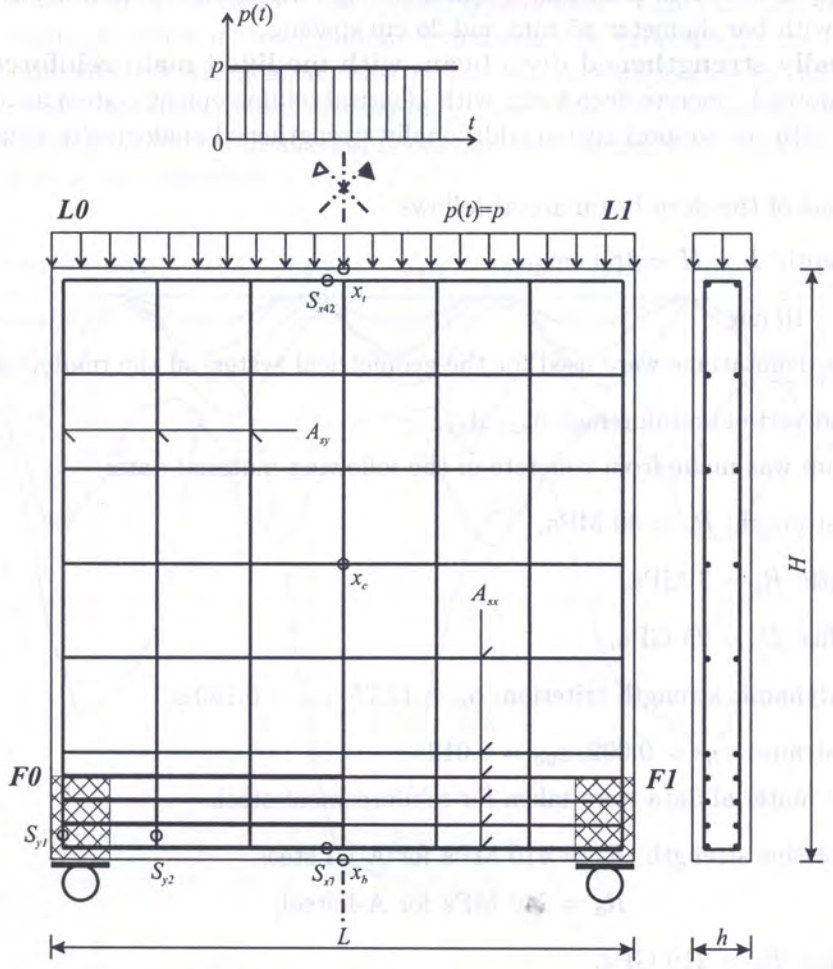

Fig. 6. Reinforced concrete deep beam under loading

The following types of the deep beams were under consideration:

***L0* – Basic deep beam**

Exactly the same rectangular reinforced concrete deep beam with orthogonal reinforcement system, as test specimen WT3 analysed in [14].

The main reinforcement consisted of A-III grade steel, in the form of 4 layers of reinforcement loops with bar diameter $\phi 8$ mm, laid at the bottom section of the beam. The upper section of the deep beam is reinforced by vertical and horizontal stirrups made from A-I grade steel, with bar diameter $\phi 5$ mm and 26 cm spacing. Mechanical properties of the smooth steel bars of A-I grade (St3SY 240/310) and the finned steel bars of A-III grade (34GS 410/500) were taken according to Polish Code.

***F0* – Additionally strengthened deep beam**
Rectangular reinforced concrete deep beam with identical reinforcement system as in the deep beam type of ***L0***, but with additionally strengthened support region. This additional strengthening was carried out analogically as in the paper by Floegl and Mang [9] and its description was presented in paper [6].

***L1* – Basic deep beam with modified main reinforcement steel**
Exactly the same rectangular reinforced concrete deep beam with orthogonal reinforcement system, as test specimen WT3 in paper [14], but with reduced main reinforcement steel.

The main reinforcement consisted of A-III grade steel, in the form of 4 layers of reinforcement loops. The first bottom loop has $\phi 8$ mm steel bar diameter and the next three loops have $\phi 5$ mm diameter. The upper section of the beam is reinforced by vertical and horizontal stirrups made from A-I grade steel, with bar diameter $\phi 5$ mm and 26 cm spacing.

***F1* – Additionally strengthened deep beam with modified main reinforcement steel**
Rectangular reinforced concrete deep beam with identical reinforcement system as in the deep beam type of ***L1***, but with the support region additionally strengthened analogically as in the deep beam type of ***F0***.

The dimensions of the deep beam are as follows:

- length and depth: $L = H = 160$ cm,
- thickness: $h = 10$ cm.

The following denotations were used for the geometrical system of the reinforcement steel:

- horizontal and vertical reinforcing: A_{sx}, A_{sy}.

The deep beam was made from concrete of the following material data:

- compressive strength: $R_c = 30$ MPa,
- tensile strength: $R_t = 3$ MPa,
- elastic modulus: $E_c = 25$ GPa,
- constants in dynamic strength criterion: $\alpha_c = 17.75$, $t_{c0} = 0.180$ s,
- limit plastic strains: $\varepsilon_{Rc} = 0.002$, $\varepsilon_{uc} = 0.012$.

The following material data were taken for reinforcement steel:

- tensile-compressive strength: $R_a = 410$ MPa for A-III steel,
  $R_a = 240$ MPa for A-I steel,
- elastic modulus: $E_a = 210$ GPa,
- viscosity coefficient: $\gamma = 40.4$ s^{-1},
- exponent coefficient in $\Phi(F)$ power function: $\delta = 5$,
- constants in dynamic yield criterion: $\alpha = 16.8$, $t_0 = 2.818$ s.

The behaviour of the presented reinforced concrete deep beam was analysed under dynamic load $p(x,t) = p = \text{const}$, uniformly distributed over the top edge, permanent in time, of different level intensities $\alpha = P/P_0$, where P is the total loading $P = p \times L$ and P_0 is the estimation of the static load-carrying capacity obtained in the numerical solution.

The estimation of the static load-carrying capacity for respective types of deep beams are as follows:

L0 – $P_0 = 1031$ kN, ***F0*** – $P_0 = 1210$ kN, ***L1*** – $P_0 = 807$ kN, ***F1*** – $P_0 = 805$ kN.

6.2. Analysis of basic deep beam

Numerical results for the ***L0*** type of deep beam are presented in the following.

In Fig. 7, variations in time of vertical displacements of point x_b at the bottom edge in the middle cross-section of the deep beam are presented for the different load levels $\alpha = P/P_0$. For load level $\alpha = 0.2$ the structure behaves elastically. Above this load level, presented displacement – time relations show inelastic symptoms of structure behaviour, which are caused by the development of inelastic and cracking processes in concrete matrix. Over the range of load level causing elastic-plastic behaviour of the deep beam, stabilisation of inelastic processes is observed. Namely, almost similar maximum and minimum amplitude of displacements appears. Moreover, this fact indicates the stability of the method of solution for the applied type of load – time function. However, for load level $\alpha = 0.6$, causing intensive material softening and cracking processes in the concrete matrix, overlapping of permanent plastic deformations in the concrete appearing in different regions of structure, is observed. This effect causes distinction between the first, the second, and the following values of maximum amplitude; stabilisation of maximum and minimum amplitudes can occur in the further periods of structure vibration.

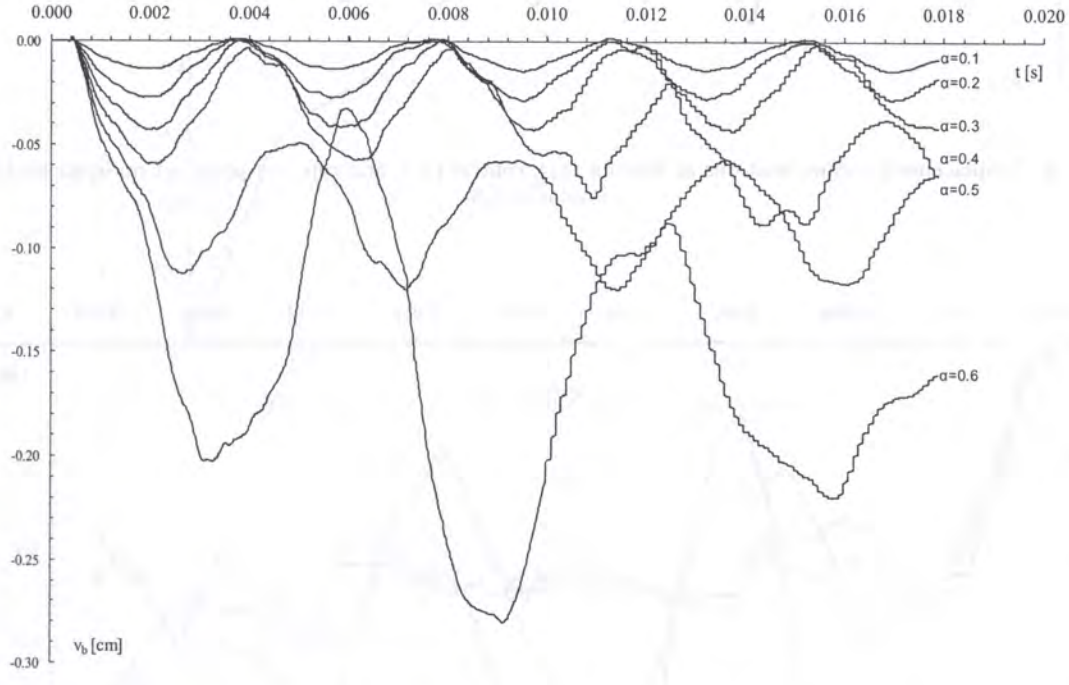

Fig. 7. Displacement – time relations for bottom (x_b) point at midspan

In the following two figures, the mutual relationship between variations in time of vertical displacements in selected points of deep beam are presented. In these figures, x_b, x_c, and x_t denote the lines describing the displacement – time relations for the bottom, central, and top layers of deep beam at midspan.

For load level $\alpha = 0.3$, *i.e.* for elastic range and for insignificant level of inelastic processes development, the results presented in Fig. 8 indicate the relationship between vertical displacements $v(x_b) < v(x_c) < v(x_t)$ well known from elastic solutions.

In turn, in Fig. 9, for load level $\alpha = 0.6$, the typical relationship between the presented displacements $v(x_b) > v(x_c) > v(x_t)$ in time intervals of attaining maximum displacement amplitudes, is observed if the intensive material softening and cracking processes in concrete matrix appears.

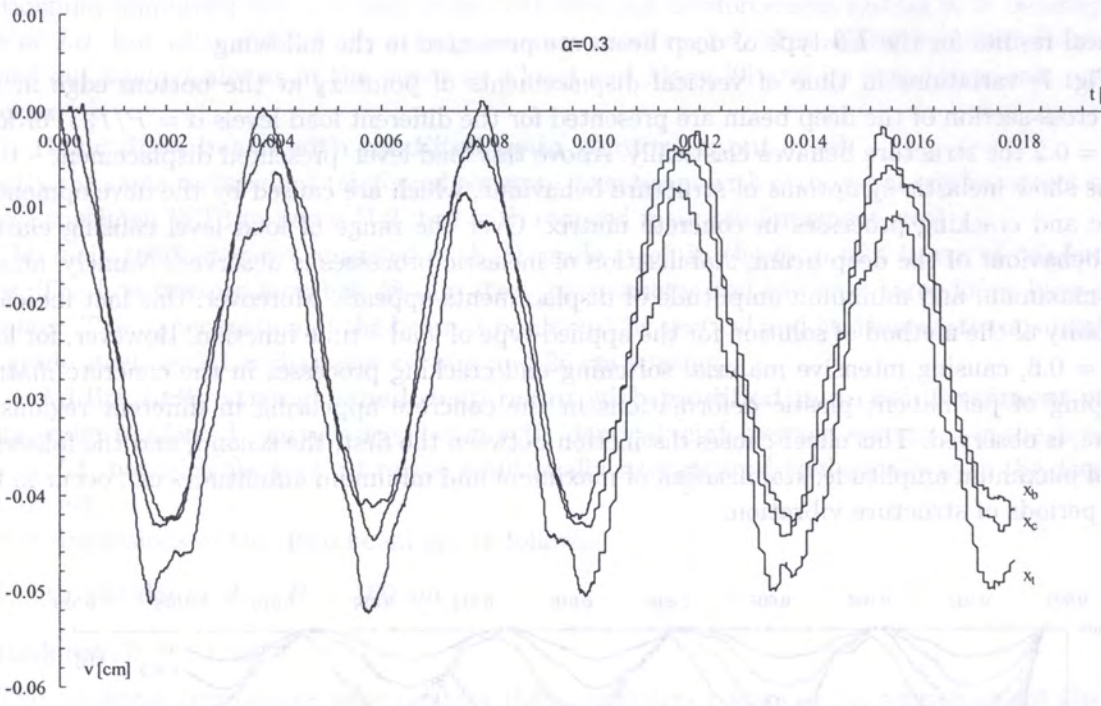

Fig. 8. Displacement – time relations at bottom (x_b), central (x_c), and top (x_t) points at midspan for load level $\alpha = 0.3$

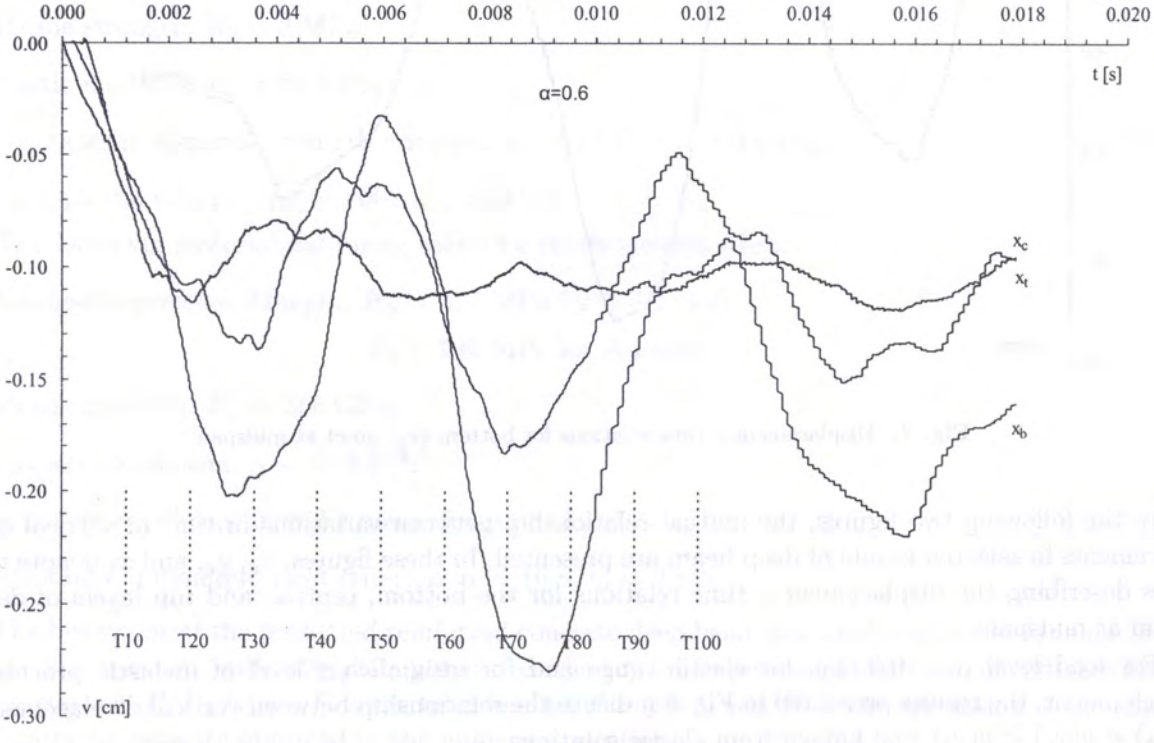

Fig. 9. Displacement – time relations at bottom (x_b), central (x_c), and top (x_t) points at midspan for load level $\alpha = 0.6$

The relationship between the permanent amplitude of vertical dynamic displacements at the point x_b and associated total load level $\alpha = P/P_0$, is presented in Fig. 10. The permanent amplitude of the displacements is determined as the equilibrium positions around which the structure demonstrates the stabilised vibrations. In the numerical solution, the permanent amplitude is practically determined at the maximum displacement rates registered between at least the second maximum and the second minimum amplitudes of displacements.

On the basis of this figure it is possible to determine the dynamic load-carrying capacity of the deep beam. The dynamic load-carrying capacity is defined as the maximum load level at which the structure demonstrates the vibrations around the equilibrium level corresponding with permanent amplitude of displacements. Further increasing of the load level caused the failure symptoms, *i.e.* disappearance of oscillations around their equilibrium positions and infinitely large increasing of the displacements.

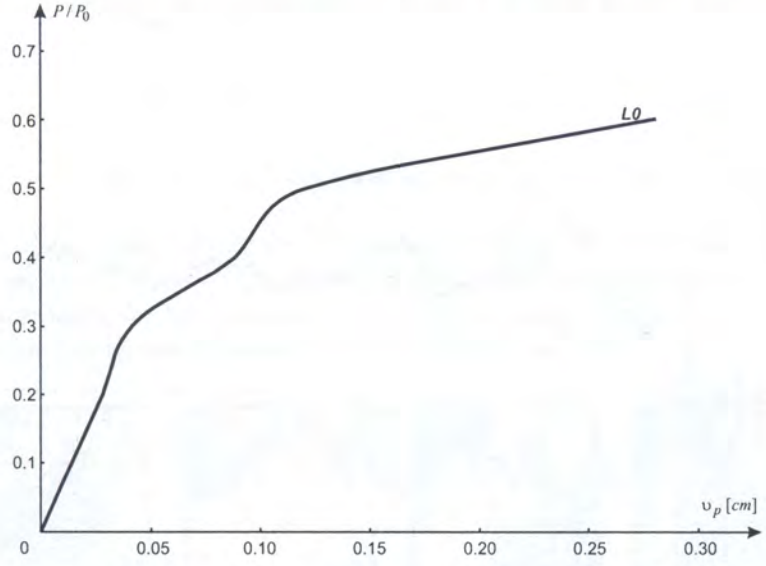

Fig. 10. Load *vs.* permanent displacement relation

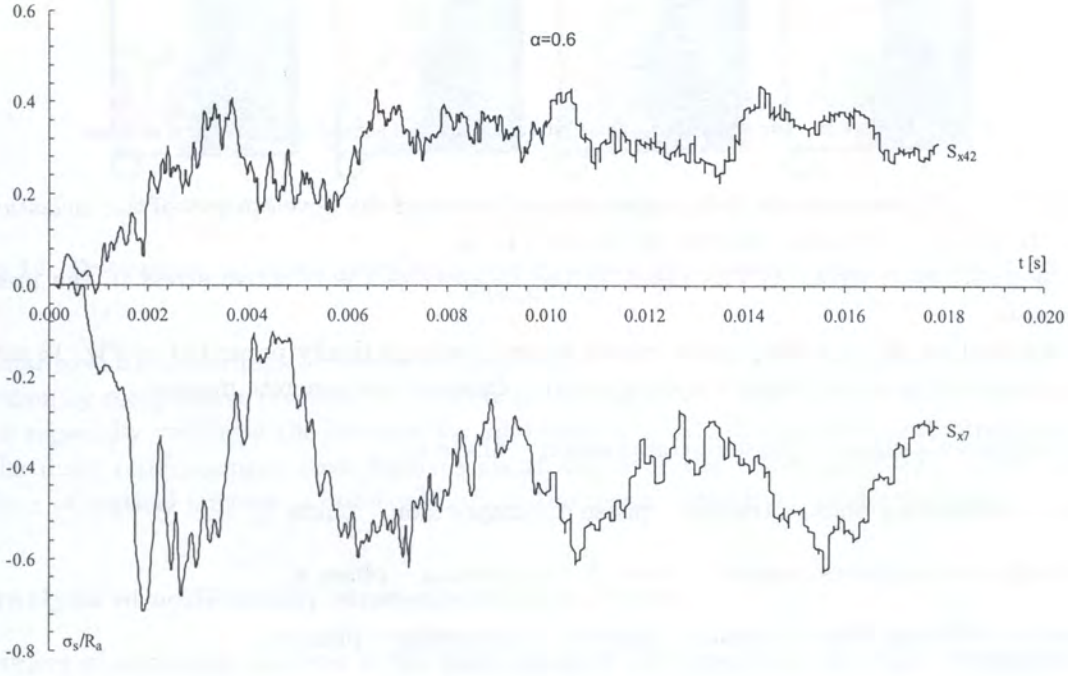

Fig. 11. Stress – time history in bottom (S_{x7}) and upper (S_{x42}) steel layers at midspan

Thus, the estimation of the load level determined as the dynamic load-carrying capacity for deep beam of type ***L0*** is $\alpha = 0.6$.

It should be underlined that despite the increasing range of cracked zones in the concrete matrix together with increasing of the load level observed in the numerical solutions, the main reinforcement steel behaves elastically over the whole range of loading.

The fact of elastic behaviour of the main reinforcement steel is confirmed in Fig. 11, in which variation in time of stresses in the bottom (S_{x7}) and upper (S_{x42}) steel layers at midspan of deep beam, is shown.

Considering the fact that the local fracture mechanism of the deep beam in the vicinity of the support occurred, the illustration of inelastic behaviour of vertical reinforcement steel bars is presented in Fig. 12. Namely, stress – time relation indicates inelastic compressive stresses at first close to the edge vertical stirrups (S_{y1}), whereas stress – time relation shows the elastic tensile behaviour of the stirrups placed directly beyond the support (S_{y2}).

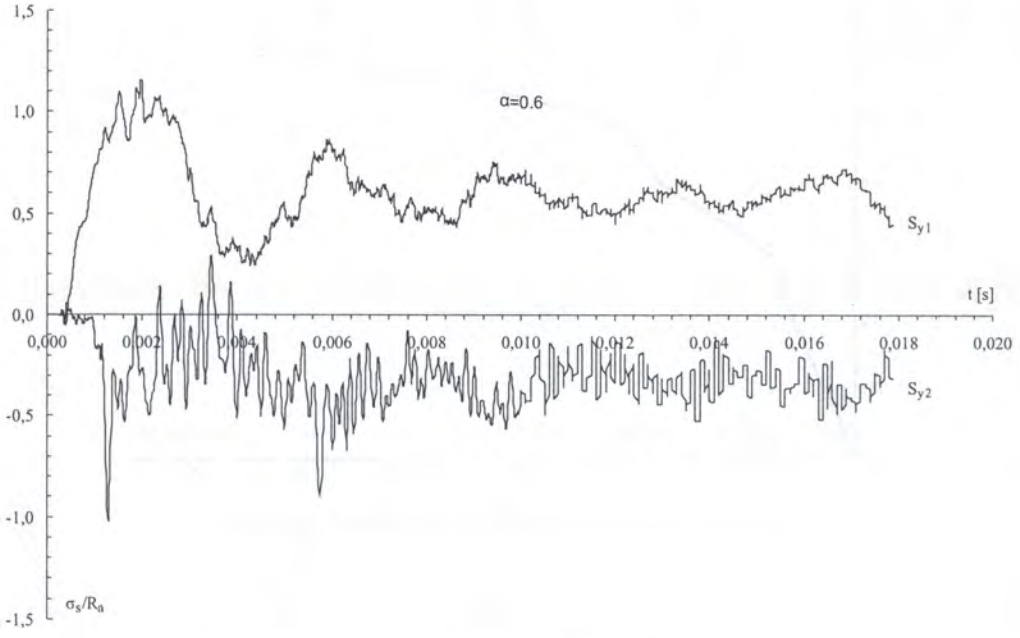

Fig. 12. Stress – time history in the first (S_{y1}) and the second (S_{y2}) vertical stirrups

The following figures provide the graphical visualisation of the development of the inelastic zones in concrete during the loading process of the deep beam.

The normal mean stress σ_0 was taken as the measure of the effective stress in the presented visualisation.

The denotation of the mean normal stress states is schematically presented in Fig. 13 with the graphical indication of the respective deformation phases of the concrete matrix:

- elastic phases: tension – phase 5, compression – phase 6,
- elastic overloading phases: tension – phase 4, compression – phase 7,
- perfectly plastic phases: tension – phase 3, compression – phase 8,
- material softening phases: tension – phase 2, compression – phase 9,
- failure phases: tension (cracking) – phase 1, compression (crushing) – phase 10.

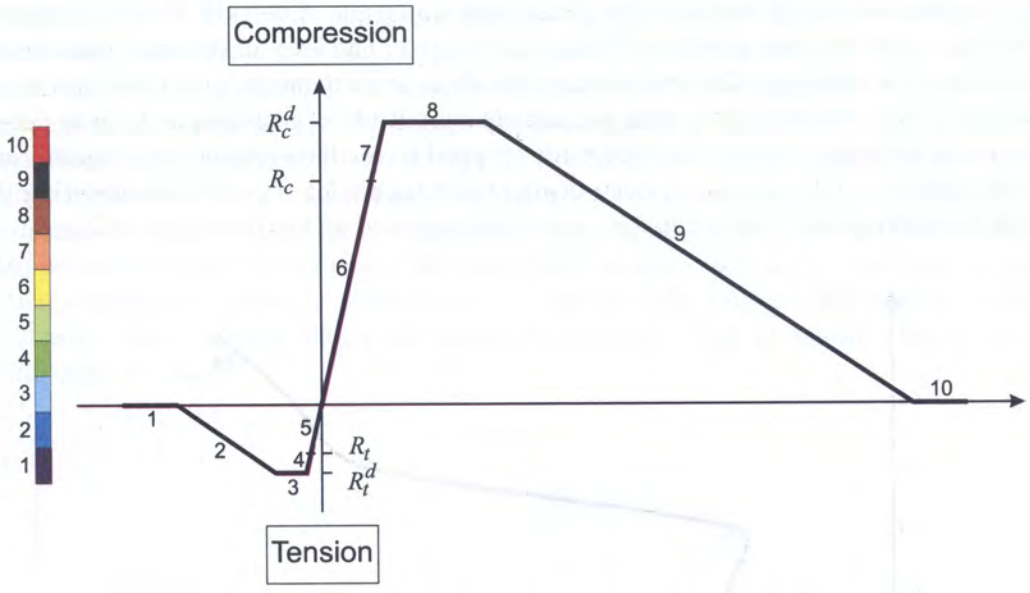

Fig. 13. Schema of mean normal stress denotation

The sequence of Figs. 14 a–d illustrates the development of the inelastic zones in the concrete matrix in selected instants of time Ti (marked in Fig. 9), until the attainment of the first maximum amplitude of displacements, for load level $\alpha = 0.6$. The presented illustrations concern the left hand half of the deep beam due to the symmetry of the structure and load.

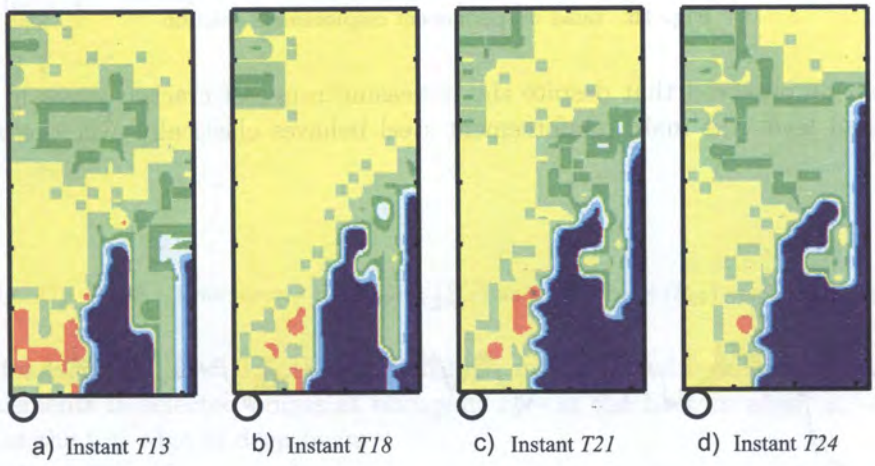

Fig. 14. Development of inelastic zones in concrete at instants $Ti = 100 \cdot i \cdot \Delta t$, ($\Delta t = 0.119 \cdot 10^{-5}$ s) for load level $\alpha = 0.6$

Similar to static experimental results [14] and numerical results [6, 7], symptoms of local fracture mechanism by compressive crushing of concrete in the region over the support can be observed. This effect is especially visible in the solution for load level $\alpha = 0.7$. It should be underlined once more that the main reinforcement steel behaves elastically over the whole range of loading. Inelastic behaviour of vertical stirrups is observed only in the region directly above the support.

6.3. Analysis of additionally strengthened deep beam

The subject of numerical analysis is the deep beam of ***F0*** type with additional strengthening in the support region.

In Fig. 15, the relationship between the permanent amplitude of vertical dynamic displacements at the point x_b and total load level $\alpha = P/P_0$, is presented. The level of dynamic load-carrying capacity, defined as the maximum loading at which the deep beam demonstrates the vibrations around the equilibrium level corresponding with permanent amplitude of displacements, was determined. In the numerical solution, vertical displacements stopped to oscillate around their equilibrium positions at load level $\alpha = 0.8$, (in case of deep beam of ***L0*** type – for $\alpha = 0.7$). Considering this fact, the level of dynamic load-carrying capacity can be determined at load level $\alpha = 0.7$.

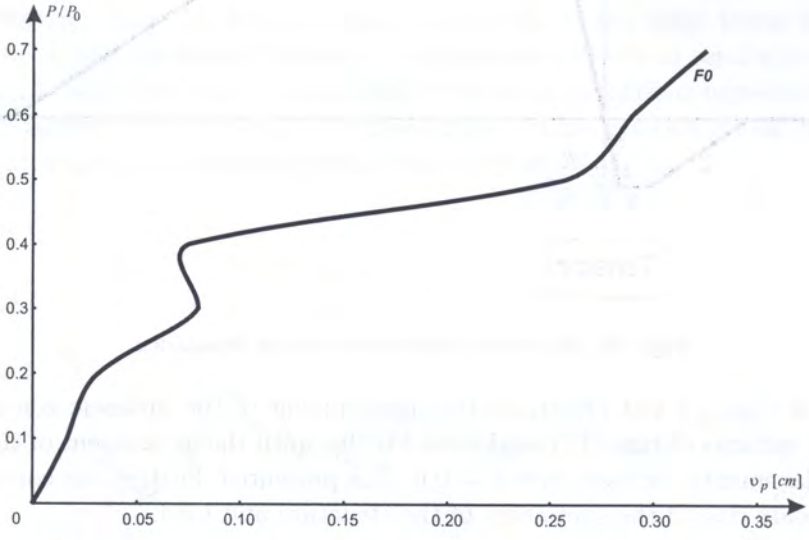

Fig. 15. Load *vs.* permanent displacement relation

Again, it can be observed that despite the increasing range of cracked zones in concrete with increasing of load level, the main reinforcement steel behaves elastically over the whole range of loading.

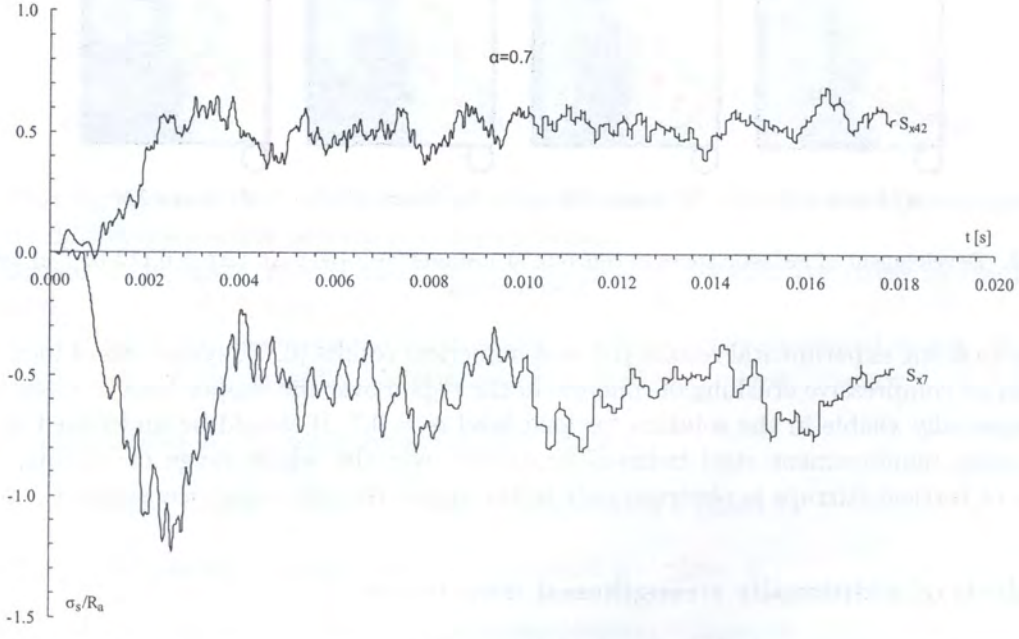

Fig. 16. Stress – time history in bottom (S_{x7}) and upper (S_{x42}) steel layers at midspan

Elastic behaviour of the main reinforcement steel is confirmed in Fig. 16, in which variation in time of stresses in the bottom (S_{x7}) and upper (S_{x42}) steel layers at midspan of deep beam, is shown. However, it can be noticed that, in the main reinforcement steel, the elastic overloading above the static strength of steel appeared. With regard to short duration character of this process, the main reinforcing steel was not subjected to viscoplastic flow process. The maximum stress equals about $1.3R_a$, while in the deep beam of ***L0*** type, the stress level did not reach the static strength of steel.

Considering the fact that the local crushing mechanism of the deep beam in the vicinity of the support appeared, inelastic behaviour of vertical reinforcement steel bars is observed. In Fig. 17, the stress – time relation indicates the viscoplastic flow at the first close to edge vertical stirrups (S_{y1}), whereas stress – time relation shows the elastic tensile behaviour of the stirrups placed directly beyond the support (S_{y2}).

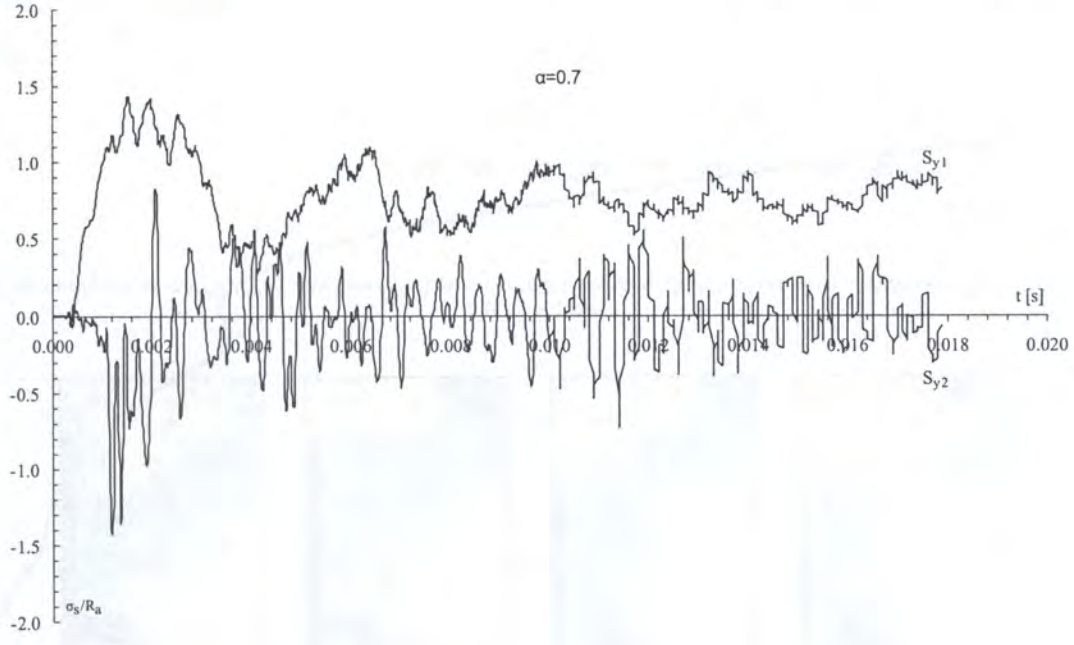

Fig. 17. Stress – time history in the first (S_{y1}) and the second (S_{y2}) vertical stirrups

In Fig. 18, for load level $\alpha = 0.7$, the relationships are presented between variations in time of vertical displacements in selected points at midspan: x_b – at the bottom edge, x_c – in the central axis, and x_t – at the top edge of deep beam.

Increase of about 20% of vertical displacements at point x_b is observed in comparison with the respective results for ***F0*** deep beam. This increase results from the changing of the stress mechanism of the deep beam, *i.e.* the additional strengthening of the support region caused the relative decrease of stiffness at midspan cross-sections. Similarly, in the case of the ***F0*** deep beam, the relationship between presented displacements $v(x_b) > v(x_c) > v(x_t)$ in time intervals of attaining the maximum displacement amplitudes, is observed.

The following sequence of Figs. 19 a–d presents the development of the inelastic zones in the concrete matrix in selected instants of time Ti (marked in Fig. 18), until the attainment of the first maximum amplitude of displacements, for load level $\alpha = 0.7$.

Numerical analysis indicates that in the additionally strengthened deep beam of ***F0*** type, a similar fracture mechanism has been observed as in the basic deep beam of ***L0*** type, but under higher load level $\alpha = 0.8$. Only slight differences in compressive crushing mechanism in the support regions were observed in comparison with ***L0*** deep beam. This fact caused the increase of the stress level at midspan region both in upper, compressive zones of concrete and in the bottom, tensile zones of

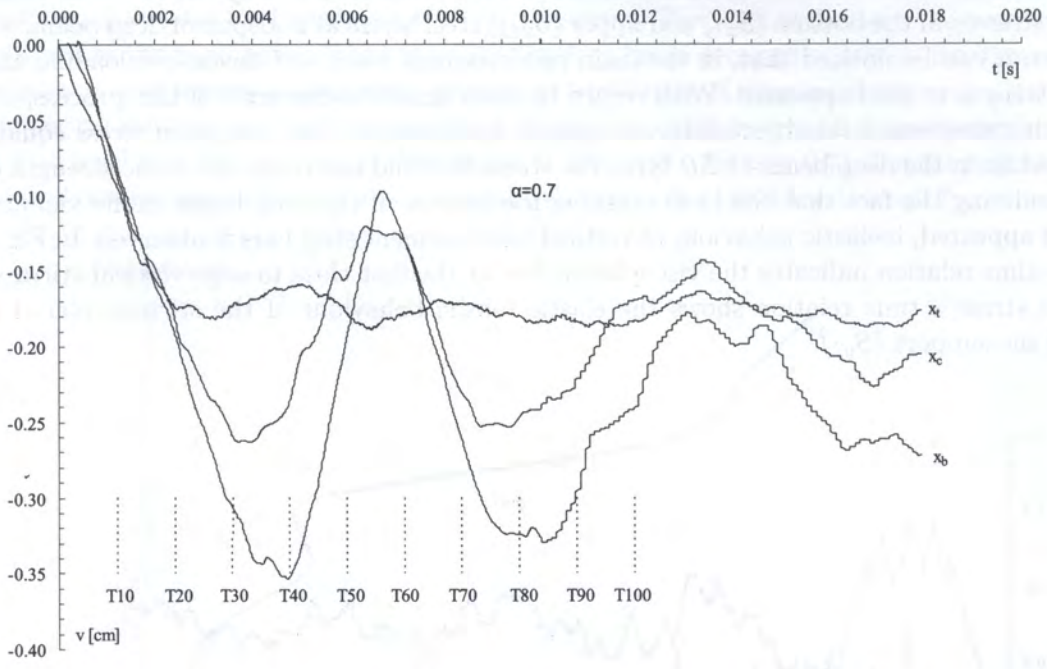

Fig. 18. Displacement – time relations at bottom (x_b), central (x_c), and top (x_t) points at midspan for load level $\alpha = 0.7$

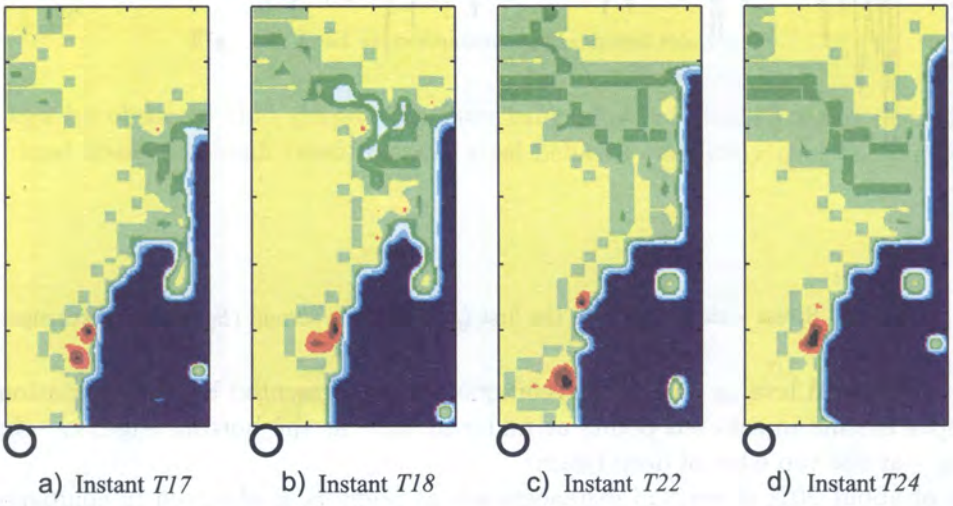

Fig. 19. Development of inelastic zones in concrete at instants $Ti = 100 \cdot i \cdot \Delta t$, ($\Delta t = 0.119 \cdot 10^{-5}$ s) for load level $\alpha = 0.7$

concrete in addition layers of main reinforcing steel. Additional strengthening of the support region caused the increase of the dynamic load-carrying capacity of the analysed deep beam. However, considering the fact that the bottom regions of the structure are over-reinforced by reinforcing steel, the dynamic load-carrying capacity was determined by the carrying capacity of the support region.

The application of the modified model of the elastic/visco-perfectly plastic material with regard to delayed yield effect to the reinforcing steel constitutive modelling, enabled the determination of the short duration process of elastic overloading above the static strength of steel in the main reinforcement. This example indicates that including the delayed yield effect in material modelling of steel behaviour, can have the qualitative influence on the change of the stress mechanism of the reinforced concrete structure.

6.4. Analysis of basic deep beam with modified main reinforcement steel

For the purpose of illustrating the influence of the inelastic behaviour of the main reinforcement steel on dynamic displacements and fracture mechanism, the numerical experiments for deep beam ***L1*** with modified quantitative and qualitative system of the main reinforcement steel were carried out.

In Fig. 20, the relationship between the permanent amplitude of vertical dynamic displacements at the point x_b and total load level $\alpha = P/P_0$, is presented. The level of dynamic load-carrying capacity, defined as the maximum loading at which the deep beam demonstrates the vibrations around the equilibrium level corresponding to permanent amplitude of displacements, was determined. In the numerical solution, the oscillations of vertical displacements around their equilibrium positions were observed to cease at load level $\alpha = 1.0$, (in cases of ***L0*** deep beam – for $\alpha = 0.7$ and of ***F0*** deep beam – for $\alpha = 0.8$).

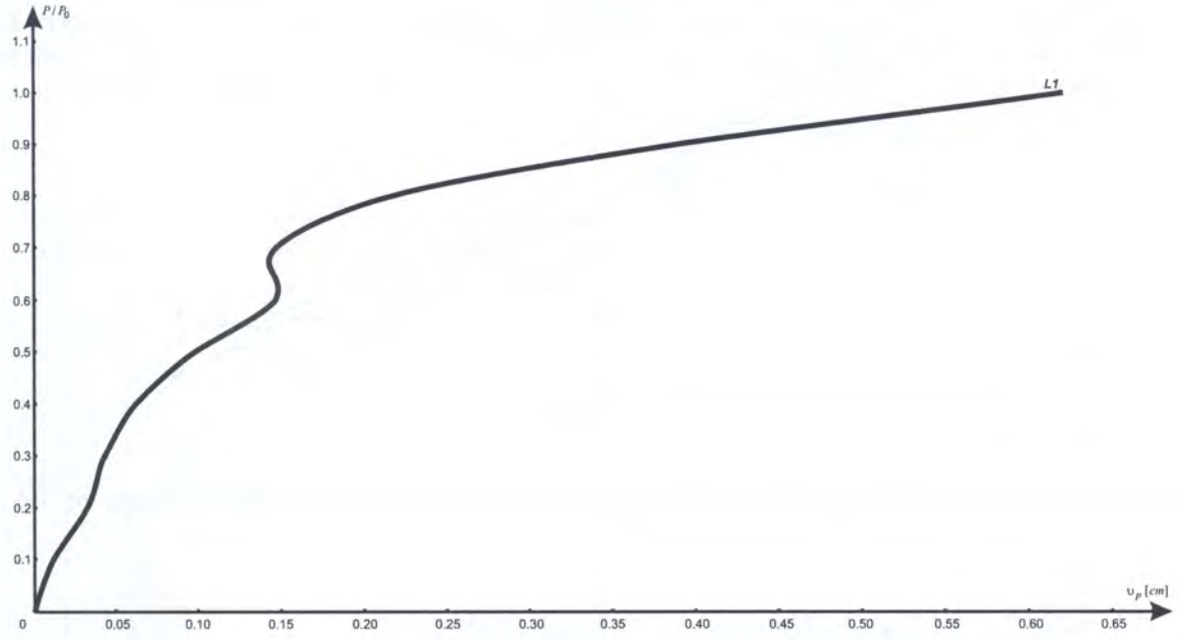

Fig. 20. Load *vs.* permanent displacement relation

In Fig. 21, for load level $\alpha = 1.0$, the relationships between variations in time of vertical displacements in selected points at midspan: x_b – at the bottom edge, x_c – in the central axis, and x_t – at the top edge of deep beam are presented.

The results indicate the typical character of displacement variation for the load level corresponding to the dynamic load-carrying capacity. Adaptation to this load level expressed by stabilisation of vibration, can occur after a very long period of time exceeding $T = 1.8{\cdot}10^{-2}$ s. Similarly, in case of the ***F0*** and ***L0*** deep beams, the relationship between presented displacements $v(x_b) > v(x_c) > v(x_t)$ in time intervals of attainment of the maximum displacement amplitudes, is observed.

The influence of the delayed yield effect of the reinforcement steel on change of stress character of the reinforced concrete deep beam, was carried out on the base on comparative analysis of numerical solutions for different material models of steel.

In Fig. 22, for load level $\alpha = 1.0$, variation in time of stresses in the bottom (S_{x7}) steel layers at midspan of deep beam is shown for two material models of reinforcing steel:

- elastic/visco-perfectly plastic model (***EV-P***),
- elastic/visco-perfectly plastic model with regard to delayed yield effect (***EV-P+DYE***).

Using **elastic/visco-perfectly plastic model** of reinforcing steel caused the typical symptoms of failure of structure in numerical solutions. Namely, 'infinitely' large values of vertical displacements are observed without appearance of any extreme values of the type of maximum or minimum amplitude of displacements. In this case, the stress level in the bottom steel layers reached values of about $1.5R_a$ only in the initial phase of structure behaviour. Then, the reinforcement steel passed into the strain state causing completely unrealistic results of the stress state.

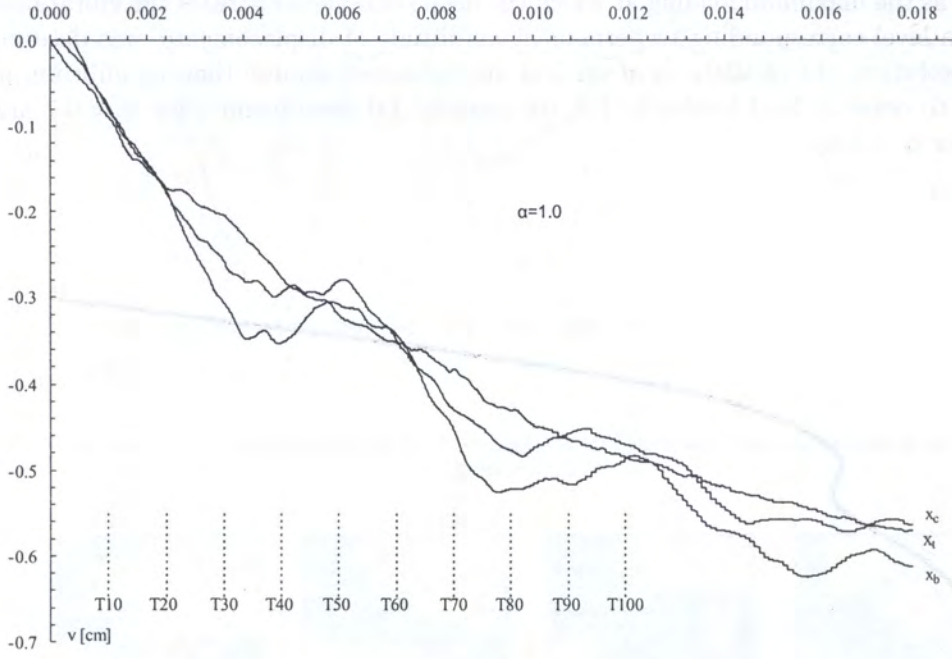

Fig. 21. Displacement – time relations at bottom (x_b), central (x_c), and top (x_t) points at midspan for load level $\alpha = 1.0$

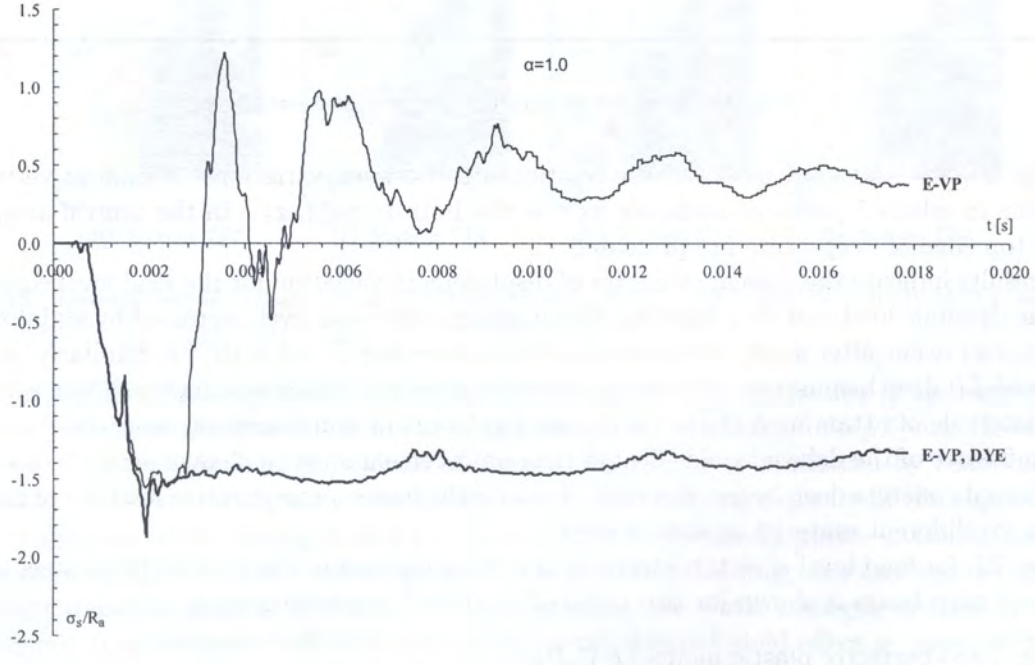

Fig. 22. Comparison of stress – time history in bottom (S_{x7}) steel layer at midspan for different material models of reinforcing steel

Application of **elastic/visco-perfectly plastic model with regard to delayed yield effect**, caused an increase of stresses until the level of about $(1.8 - 1.9)R_a$ in the elastic overloading process, and then stabilisation of viscoplastic flow process at the stress level of about $1.5R_a$. The analysis indicates that just this 25% increase of stress level in the elastic overloading process decided that the stressing process has been taken over by steel in the support region in which the concrete was cracked. During further process of deformation, the zones of critical stress state of structure moved to the midspan regions, what, in consequence, caused the local crushing of compressive concrete in the upper zones in the midspan.

The presented solution indicates that taking into consideration the delayed yield effect in the constitutive model of steel can have a qualitative influence on the stress mechanism and dynamic load-carrying capacity. In the numerical solution, without regard to the delayed yield effect in the steel model, typical symptoms of failure of the structure are observed for load level $\alpha = 1.0$. Therefore, the dynamic load-carrying capacity for the deep beam in this type of solution should be accepted on load level $\alpha = 0.9$. For this load level, variation in time of stresses in the bottom (S_{x7}) and upper (S_{x42}) steel layers at midspan of the deep beam is shown in Fig. 23. Now, a typical, stabilised character of stress history in the bottom steel layer is observed. Such a character of stress history indicates adaptation to the given load level.

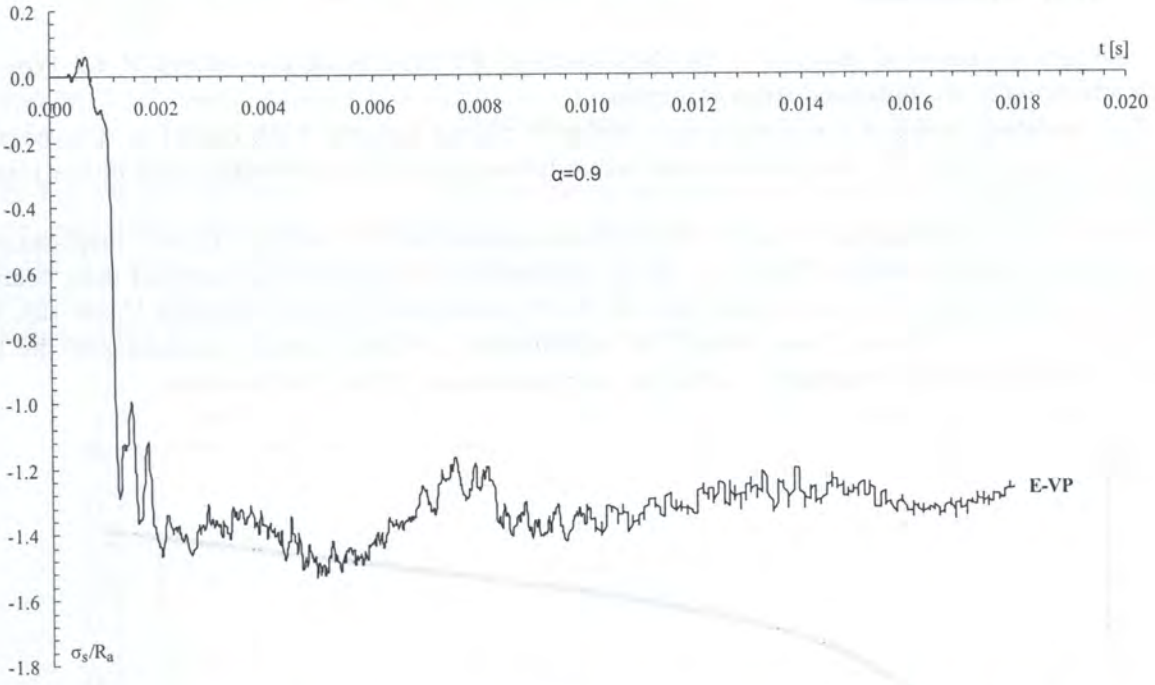

Fig. 23. Stress – time history in bottom (S_{x7}) steel layer at midspan for elastic/visco-perfectly plastic model of steel

In the following group of Figs. 24 a–d, the development of the inelastic zones in the concrete matrix in selected instants of time Ti (marked in Fig. 21), is presented for load level $\alpha = 1.0$

Numerical analysis indicates that in the deep beam of ***L1*** type, different fracture mechanisms have been realised as in the deep beams of ***L0*** and ***F0*** types. The quantitative and qualitative reduction of the main reinforcement steel system, caused both a change of the fracture mechanism and an increase of the dynamic load-carrying capacity of the deep beam. In the case of ***L0*** and ***F0*** deep beams, the local crushing mechanism in concrete occurred in the vicinity of the support region. In the case of ***L1*** deep beam, the local crushing mechanism in concrete appeared in the upper, compressive midspan zone, in the typical way for the so called beam failure mechanism.

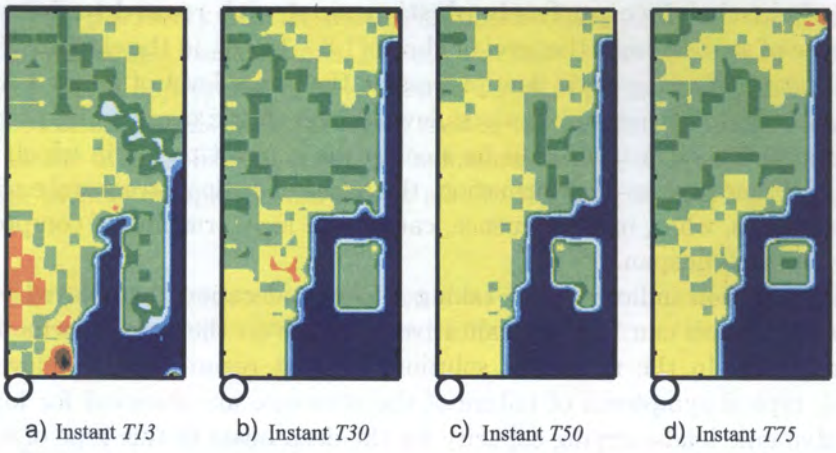

Fig. 24. Development of inelastic zones in concrete at instants $Ti = 100 \cdot i \cdot \Delta t$, ($\Delta t = 0.119 \cdot 10^{-5}$ s) for load level $\alpha = 1.0$

6.5. Analysis of additionally strengthened deep beam with modified main reinforcement steel

The subject of numerical analysis is the deep beam of ***F1*** type being the variant of ***L1*** type but with additionally strengthened support region.

The modified model of the elastic/visco-perfectly plastic material with regard to delayed yield effect was applied for the description of dynamic behaviour of the reinforcing steel in the present numerical analysis.

In Fig. 25, the relationship between the permanent amplitude of vertical dynamic displacements at the point x_b and total load level $\alpha = P/P_0$, is presented. In case of the analysed deep beam of ***F1*** type, load level $\alpha = 1.0$ was determined as the dynamic load-carrying capacity. Under this load level the structure still oscillates around the equilibrium position. Further increasing of the load level caused the failure symptoms – infinitely large increasing of the displacements.

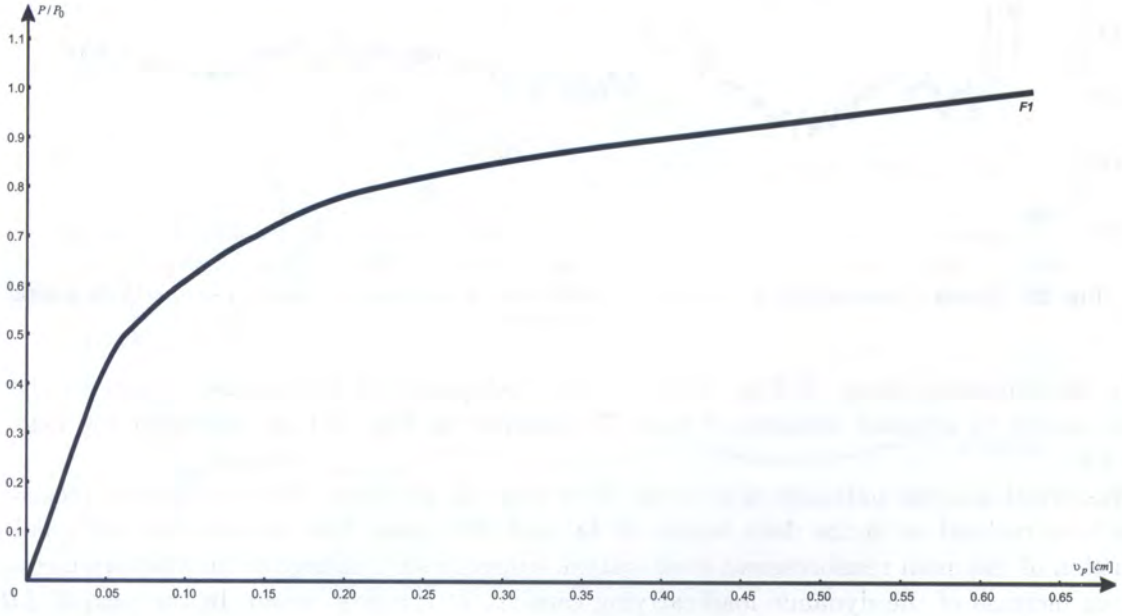

Fig. 25. Load *vs.* permanent displacement relation

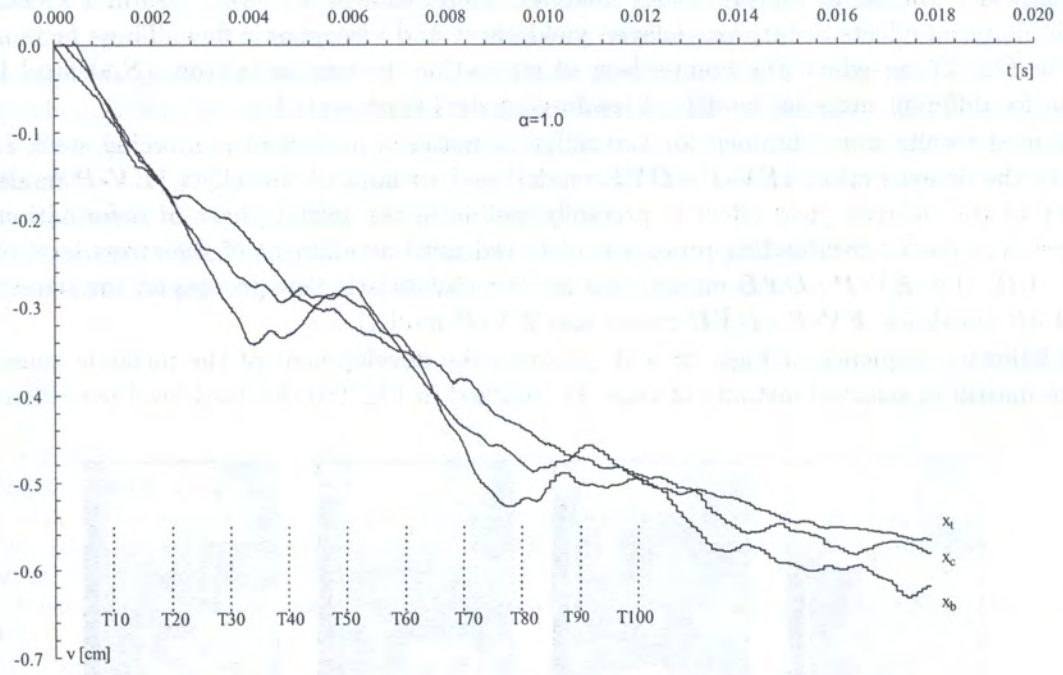

Fig. 26. Displacement – time relations at bottom (x_b), central (x_c), and top (x_t) points at midspan for load level $\alpha = 1.0$

In Fig. 26, for load level $\alpha = 1.0$, the relationships between variations in time of vertical displacements in selected points at midspan: x_b – at the bottom edge, x_c – in the central axis, and x_t – at the top edge of deep beam are presented. Similarly, in the case of the deep beams analysed previously, the relationship between presented displacements $v(x_b) > v(x_c) > v(x_t)$ in time intervals of attaining the maximum displacement amplitudes, is observed.

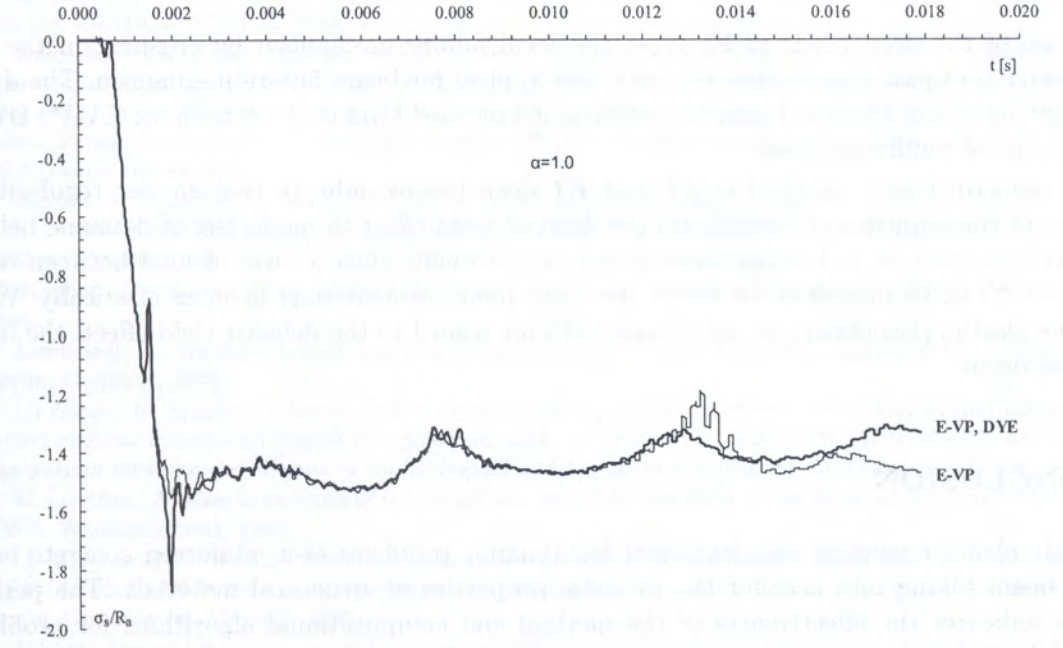

Fig. 27. Comparison of stress – time history in bottom (S_{x7}) steel layer at midspan for different material models of reinforcing steel

Analogically, similar to the previously analysed deep beam of ***L1*** type, also in ***F1*** deep beam dynamic material effects occur, *i.e.* delayed yield effect and viscoplastic flow. These facts are confirmed in Fig. 27, in which the comparison of stress-time history in bottom (S_{x7}) steel layer at midspan for different material models of reinforcing steel is presented.

Presented results were obtained for two different material models of reinforcing steel, *i.e.* with regard to the delayed effect (***EV-P+DYE*** model) and without of this effect (***EV-P*** model). The influence of the delayed yield effect is precisely visible in the initial phase of deformation of the structure. The elastic overloading process is observed until attainment of the stress level of about $(1.8 - 2.0)R_a$ (for ***EV-P+DYE*** model) and further viscoplastic flow process on the stress level of about $1.5R_a$(both for ***EV-P+DYE*** model and ***EV-P*** model).

The following sequence of Figs. 28 a–d, presents the development of the inelastic zones in the concrete matrix in selected instants of time Ti (marked in Fig. 26), for load level $\alpha = 1.0$.

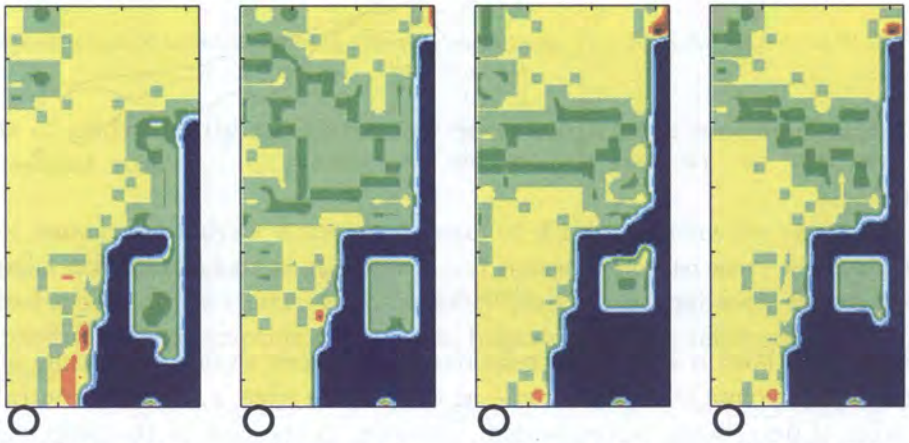

Fig. 28. Development of inelastic zones in concrete at instants $Ti = 100 \cdot i \cdot \Delta t$, $(\Delta t = 0.119 \cdot 10^{-5} s)$ for load level $\alpha = 1.0$

In case of the deep beam of F1 type, the local failure mechanism by crushing in the upper, compressive midspan zone is observed, in a way typical for beam failure mechanism. The dynamic load-carrying of the F1 deep beam was determined on load level $\alpha = 1.0$ both for EV-P+DYE and EV-P model of reinforcing steel.

The numerical analyses for the ***L1*** and ***F1*** deep beams indicate that similar regularities are observed of the sequence of considering the delayed yield effect in modelling of dynamic behaviour of reinforcing steel as in homogeneous structures. Namely, such a level of load between $\alpha = 0.3$ and $\alpha = 0.4$ can be indicated for which the main reinforcement steel behaves elastically. Whereas using the elastic/viscoplastic model of steel without regard to the delayed yield effect, the inelastic processes occur.

7. CONCLUSION

The finite element method was developed for dynamic problems of a reinforced concrete beam or a deep beam taking into account the inelastic properties of structural materials. The performed analysis indicates the effectiveness of the method and computational algorithms for problems of numerical simulation of reinforced concrete structures dynamic behaviour.

The comparative analysis of numerical results with experimental and other theoretical results known from literature was presented for dynamics of the reinforced concrete beam modelled as the

plane stress problem. The comparisons of the obtained results emphasise the accuracy of applied assumptions and deformation models of concrete and reinforcement steel.

The applied constitutive models of the materials (especially for the concrete) have the fundamental influence on the character of the stress distribution. The stress state was illustrated in the form of the scheme of the mean normal stress distribution on the surface of the deep beam. The final distribution of the stress state of the deep beam indicates the qualitative consistency with the failure mechanism observed during the static experiment.

It is also worth underlining that the dynamic load-carrying capacity for the over-reinforced main reinforcing steel deep beams types of ***L0*** and ***F0*** is less than static one.

References

[1] G. Bąk, A. Stolarski. Delayed yield effect in dynamic flow of elastic/visco-perfectly plastic material. *Arch. Mech.*, **37**: 4–5, 285–302, 1985.

[2] G. Bąk, A. Stolarski. Nonlinear analysis of reinforced concrete beams under impulsive load. I – Discretisation of the reinforced concrete beam dynamic problem. II – Numerical analysis and comparison with experimental results. *Engineering Transactions*, **36**, 3, I: 501–512, II: 519–539, 1988.

[3] O. Buyukozturk. Nonlinear analysis of reinforced concrete structures. *Computers and Structures*, **7**: 149–156, 1977.

[4] J. D. Campbell. The dynamic yielding of mild steel. *Acta Metallurgica*, **1**: 706–710, 1953.

[5] W. Cichorski, A. Stolarski. Sensitivity of the numerical solution to finite element mesh for reinforced concrete deep beams. *Computer Assisted Mechanics and Engineering Sciences*, **7**: 195–206, 2000.

[6] W. Cichorski, A. Stolarski. Analysis of displacement state of the inelastic reinforced concrete deep beam under static load *Bulletin of Military University of Technology*, L, 5(585), 5–19, 2001.

[7] W. Cichorski, A. Stolarski. Analysis of stress state of the inelastic reinforced concrete deep beam under static load. *Bulletin of Military University of Technology*, L, 5(585), 21–45, 2001.

[8] F. Emrich, J. Herter, G. Puffer. Nonlinear finite element analysis of reinforced concrete beams under impact loads in comparison with experimental results. *Proceedings RILEM-CEB-IABSE-IAAS-Interassotiation Symposium on Concrete Structures Under Impact and Impulsive Loading*, Berlin, Germany, II, 455–471, 1982.

[9] H. Floegl, H. Mang. Tension stiffening concept based on bond slip. *Journal of the Structural Division.* Proc. ASCE, 108, ST12, 2681–2701, 1982.

[10] J. Ghaboussi, W. A. Millavec, J. Isenberg. R/C structures under impulsive loading. *Journal of Structural Engineering*, vol.110, **3**: 505–522, 1984.

[11] J. Karolak, A. Winnicki. Simulations of dynamics response of concrete structures using viscoplastic Hoffmann consistency model. *Proceedings of the Fifth World Congress on Computational Mechanics (WCCM V)*, July 7-12, 2002, Vienna, Austria, H.A. Mang, F.G. Rammerstorfer, J. Eberhardsteiner. Editors: Publisher: Vienna University of Technology, Austria, ISBN 3-9501554-2-2, RS 103.2, II-420; ISBN 3-9501554-0-6, http://wccm.tuwien.ac.at.

[12] J. Karolak, A. Winnicki. Dynamic analysis of concrete structures using viscoplastic Hoffmann consistency model. 4-th *International Conference on Analytical Models and New Concepts in Concrete and Masonry Structures.* Kraków, Poland, June 5–7, 60–65, 2002.

[13] M. Kleiber, *The finite element method in nonlinear continuum mechanics*(in Polish). PWN, Warsaw, Poland, 1985.

[14] F. Leonhardt, R. Walther. *Wandartige träger* (in German). Report. Deutscher Ausschüβ für Stahlbeton, 229, Berlin, Germany, 1966.

[15] E. Limberger, K. Brandes, J. Herter. Influence of mechanical properties of reinforcing steel on the ductility of reinforced concrete beams with respect to high strain rates. *Proceedings RILEM-CEB-IABSE-IAAS-Interassotiation Symposium on Concrete Structures Under Impact and Impulsive Loading*, Berlin, Germany, II, 134–145, 1982.

[16] P. M. Lewiński. *Nonlinear analysis of reinforced concrete slabs and disks by the finite element method* (in Polish). PWN, Warszawa-Łódź, 1990.

[17] M. J. Mikkola, H. S. Sinsalo. Nonlinear dynamic analysis of reinforced concrete structures. *Proceedings RILEM-CEB-IABSE-IAAS-Interassotiation Symposium on Concrete Structures Under Impact and Impulsive Loading*, Berlin, Germany, II, 534–547, 1982.

[18] L. Nilsson. *Impact loading on concrete structures.* Chalmers University of Technology, Department of Structural Mechanics, Publ. 79:1, Göteborg, 1979.

[19] P. Perzyna. The constitutive equations for rate sensitive plastic materials. *Quart. Appl. Math.*, **20**: 321–332, 1963.

[20] H. Reimann. *Kritische Spannunszustände des Betons bei mehrachsiger, ruhender Kurzzeitbelastung* (in German). Deutscher Ausschüβ für Stahlbeton, 175, Berlin, Germany, 1965, .

[21] A. Stolarski. Model of dynamic deformation of concrete (in Polish). *Archives of Civil Engineering*, XXXVII, (3–4): 405–447, 1991.

[22] A. Stolarski, W. Cichorski. Nonlinear Analysis of Reinforced Concrete Beams and Deep Beams under Impulsive Load. *Proceedings of the 3*-rd *Asia-Pacific Conference on Shock & Impact Loads on Structures*, Singapore, 453 – 460, 24–26 November 1999.

[23] A. Stolarski, W. Cichorski. The method of analysis of the inelastic behaviour of the reinforced concrete deep beam under dynamic load (in Polish). *Bulletin of Military University of Technology*, L, 6(586), 35–68, 2001.

[24] K. J. Willam, E. P. Warnke. Constitutive model for the triaxial behavior of concrete. *Int. Ass. for Bridge and Struct. Engng., Seminar on Concrete Structures Subjected to Triaxial Stresses*, Bergamo, Italy, III-1, 1–30, 1974.

[25] O. C. Zienkiewicz. *The finite element method.* (in Polish) McGraw-Hill, London, England, 1977, [Arkady, Warsaw, Poland, 1972].